NASA TECHNICAL NOTE

NASA TN D-6895

NASA TN D-6895

NUMERICAL ANALYSIS OF THE TRANSIENT RESPONSE OF AN AXISYMMETRIC ABLATIVE CHAR LAYER CONSIDERING INTERNAL FLOW EFFECTS

by Claud M. Pittman and Lona M. Howser

Langley Research Center
Hampton, Va. 23365

NATIONAL AERONAUTICS AND SPACE ADMINISTRATION • WASHINGTON, D. C. • SEPTEMBER 1972

1. Report No.	2. Government Accession No.	3. Recipient's Catalog No.
NASA TN D-6895		

4. Title and Subtitle	5. Report Date
NUMERICAL ANALYSIS OF THE TRANSIENT RESPONSE OF AN AXISYMMETRIC ABLATIVE CHAR LAYER CONSIDERING INTERNAL FLOW EFFECTS	September 1972
	6. Performing Organization Code
7. Author(s)	8. Performing Organization Report No.
Claud M. Pittman and Lona M. Howser	L-7868
	10. Work Unit No.
9. Performing Organization Name and Address	502-37-02-01
NASA Langley Research Center Hampton, Va. 23365	11. Contract or Grant No.
	13. Type of Report and Period Covered
12. Sponsoring Agency Name and Address	Technical Note
National Aeronautics and Space Administration Washington, D.C. 20546	14. Sponsoring Agency Code

15. Supplementary Notes

16. Abstract

The differential equations governing the transient response of the char layer of an ablating axisymmetric body, internal pyrolysis gas flow effects being considered, have been derived. These equations have been expanded into finite-difference form and programed for numerical solution on a digital computer. Numerical results compare favorably with simplified exact solutions.

The complete numerical analysis was used to obtain solutions for two representative body shapes subjected to a typical entry heating environment. Pronounced effects of the lateral flow of pyrolysis gases on the mass flow field within the char layer and the associated surface and pyrolysis interface recession rates are shown.

17. Key Words (Suggested by Author(s))	18. Distribution Statement
Ablation Char layer Axisymmetric numerical analysis	Unclassified – Unlimited

19. Security Classif. (of this report)	20. Security Classif. (of this page)	21. No. of Pages	22. Price*
Unclassified	Unclassified	61	$3.00

*For sale by the National Technical Information Service, Springfield, Virginia 22151

NUMERICAL ANALYSIS OF THE TRANSIENT RESPONSE OF AN AXISYMMETRIC ABLATIVE CHAR LAYER CONSIDERING INTERNAL FLOW EFFECTS

By Claud M. Pittman and Lona M. Howser
Langley Research Center

SUMMARY

The differential equations governing the transient response of the char layer of an ablating axisymmetric body, internal pyrolysis gas flow effects being considered, have been derived. These equations have been expanded into finite-difference form and programed for numerical solution on a digital computer. Numerical results compare favorably with simplified exact solutions.

The complete numerical analysis was used to obtain solutions for two representative body shapes subjected to a typical entry heating environment. Pronounced effects of the lateral flow of pyrolysis gases on the mass flow field within the char layer and the associated surface and pyrolysis interface recession rates are shown.

INTRODUCTION

One-dimensional ablation analyses have been used extensively to study the thermal response of charring ablator heat shields subjected to aerodynamic heating. Recent experimental results, both in ground and flight test, show that a two-dimensional effect, involving the lateral flow of pyrolysis gases within the char layer, can significantly affect the performance of ablative materials. (See refs. 1 and 2.) This phenomenon becomes important in heat-shield areas such as stagnation regions and leading edges which have relatively sharp radii of curvature, high heating rates, and large surface-pressure gradients. The high heating rates produce thick char layers and, because of the large surface-pressure gradients, the pyrolysis gases within the char layer tend to develop a significant lateral flow component. Because of this lateral flow, the mass of pyrolysis gas injected into the boundary layer is reduced in some areas and increased in others and this condition affects both blocking of convective heating and surface recession.

One-dimensional ablation analyses, such as that described in reference 3, can be modified with factors obtained from exact solutions for simplified two-dimensional flow fields. Such a procedure (which was used in ref. 1) is useful but does not provide any

assessment of the accuracy of the results that are obtained. Clearly, a two-dimensional analysis of heat and mass transfer within a char layer is needed. Several two-dimensional thermal analyses are available. (See refs. 4 to 10.) Of these, only reference 9 attempts to treat the pyrolysis gas flow field within a charring ablator. In reference 9, only the energy and continuity equations are solved and the simplifying assumption is made that the gas mass flow rate vector in the char is oriented with the temperature-gradient vector rather than with the pressure-gradient vector.

This paper presents an analysis which determines both the temperature and pressure fields within the char layer. The analysis considers (1) the effect of two-dimensional mass flow on the temperature distribution and recession rates and (2) the effect of temperature on the pressure and, therefore, on the mass flow distribution. The analysis is transient and is programed in terms of general curvilinear coordinates.

The governing differential equations are derived and are converted to finite-difference form by using Taylor's series expansions. An acceptable method of solution for the finite-difference equations was difficult to find. The method which was finally used to obtain solutions was to solve implicitly through the thickness of the char layer and explicitly along the other coordinate. This method is stable when the gradients through the thickness are dominant and yielded several solutions of interest. A method of solution which is always stable was not found.

As the numerical solution is time consuming at best, and unstable under certain conditions, a criterion (based on a simplified two-dimensional exact solution and a one-dimensional numerical analysis) is presented which can be used to identify conditions where lateral internal mass transfer will be significant.

Numerical results compare favorably with exact solutions for simplified cases. Solutions are also shown for two body shapes, subjected to a typical ballistic entry environment, to illustrate the significant effects of two-dimensional mass flow.

SYMBOLS

A	quantity defined by equation (3)
A_i, A_s	constants in mass loss rate equations corresponding to specific reaction rate
B	dummy variable used in appendix D
B_i, B_s	constant in exponential of mass loss rate equation corresponding to activation energy

C	constant used in exact solution (see eq. (D1))
C_e	oxygen concentration by mass at edge of boundary layer
c_p	specific heat of char
$\bar{c}_p$	specific heat of pyrolysis gases
f	porosity of char
h	enthalpy
h_1,h_2,h_3	scale factors given by equations (A5)
Δh_c	heat of combustion
Δh_p	heat of pyrolysis
K	reaction-rate constant for char oxidation
k	thermal conductivity of char
L	total distance along base curve (fig. 2)
M	molecular weight of gases
$\dot{m}$	mass flow rate
p	pressure
q	heating rate
R	radius of curvature
R_o	universal gas constant
R_1,R_2	radii (defined after eq. (D8))
R_s	normal distance from axis to base curve (fig. 2)

$R_{\psi,r}$	radius (defined after eq. (D8))
r	dimensionless radius (eq. (D8))
s	arc length
T	temperature
v	velocity
x,y,θ	coordinates
$y_{p,o}$	distance from base curved to pyrolysis interface
α	absorptance of char surface
α_s	weighting factor for transpiration effectiveness
β	angle between tangent to base curve and axis of symmetry (fig. 2)
γ	angle defined in figure 3
δ	char thickness
ϵ	emittance of char surface
η	transformed y-coordinate
κ	permeability
λ	mass of char removed per unit mass of oxygen
μ	viscosity
ρ	density of char
ρ'	density of uncharred material
σ	Stefan-Boltzmann constant

τ	time
φ	quantity defined by equation (12)
ψ	angle in spherical coordinates (eq. (D8))

Subscripts:

C	cold-wall convective
C,net	hot-wall convective heating corrected for transpiration
c	char
e	at edge of boundary layer
g	gas
o	initial
p	pyrolysis interface
R	radiative
s	char surface
t	stagnation point
w	wall
x	x-component
y	y-component
1-D	one-dimensional
2-D	two-dimensional

An arrow over a symbol denotes a vector.

ANALYSIS

A transient analysis is developed for an axisymmetric char layer (fig. 1) subjected to a typical entry heating environment. The primary result sought is the effect of axisymmetric temperature and pressure distributions on the mass flow within the char layer and on the char surface and pyrolysis interface recessions. Although only the char layer was analyzed, the back surface of the uncharred material was used as the base curve for the coordinate system, since it always remained fixed.

Assumptions

The primary assumptions used in the analysis are as follows:

(1) The density of the char layer is constant.

(2) The thermal conductivity of the char layer is a function of temperature only.

(3) The permeability of the char layer is a function of temperature and direction.

(4) The heat transfer and pyrolysis gas flow are zero normal to the surfaces $x = 0$ and $x = L$. (See fig. 2.)

(5) Char surface removal is by oxidation only.

(6) The effect of surface shape changes on surface heating rates and pressures are neglected.

(7) The gradients in the θ-direction are zero.

Differential Equations for the Temperature Distribution

Governing temperature equation.- The governing equation for the temperature distribution in the char layer in vector form is

$$\underbrace{\nabla \cdot k\nabla T}_{\substack{\text{Heat} \\ \text{conducted}}} - \underbrace{\nabla \cdot \left(\vec{m}\bar{c}_p T\right)}_{\substack{\text{Heat absorbed by} \\ \text{pyrolysis gases}}} = \underbrace{\frac{\partial}{\partial \tau}\left[\left(\rho c_p + \rho_g \bar{c}_p\right)T\right]}_{\substack{\text{Heat} \\ \text{stored}}} \tag{1}$$

The development of equation (1) into the form to be used in the analysis is given in appendix A. Through this development, equation (1) becomes

$$\frac{\partial}{\partial x}\left(\frac{h_2}{h_1} k \frac{\partial T}{\partial x}\right) - \frac{\partial}{\partial x}\left(\frac{h_2}{h_1} kA \frac{\partial T}{\partial \eta}\right) - A \frac{\partial}{\partial \eta}\left(\frac{h_2}{h_1} k \frac{\partial T}{\partial x}\right) + A \frac{\partial}{\partial \eta}\left(\frac{h_2}{h_1} kA \frac{\partial T}{\partial \eta}\right)$$

$$+ \frac{1}{\delta^2} \frac{\partial}{\partial \eta}\left(h_1 h_2 k \frac{\partial T}{\partial \eta}\right) - h_2 \dot{m}_x \frac{\partial}{\partial x}\left(\bar{c}_p T\right) + h_2 A \dot{m}_x \frac{\partial}{\partial \eta}\left(\bar{c}_p T\right) - \frac{h_1 h_2 \dot{m}_y}{\delta} \frac{\partial}{\partial \eta}\left(\bar{c}_p T\right)$$

$$= h_1 h_2 \rho c_p \frac{\partial T}{\partial \tau} + \frac{h_1 h_2 c_p \eta \dot{m}_c}{\delta} \frac{\partial T}{\partial \eta} + \frac{h_1 h_2 (1 - \eta) \dot{m}_p \rho c_p}{\delta(\rho' - \rho)} \frac{\partial T}{\partial \eta} \quad (2)$$

where

$$A = \frac{1}{\delta}\left(\eta \frac{\partial \delta}{\partial x} + \frac{\partial y_p}{\partial x}\right) \quad (3)$$

$$\eta = \frac{y - y_p}{\delta} \quad (4)$$

and h_1 and h_2 are scale factors, shown in figure 3 and discussed in appendix A.

Initial conditions.- The initial conditions that must be specified are the temperature distribution, mass-transfer rates, and the body shape. For most cases of interest, the initial temperature distribution is uniform and the initial mass-transfer rate is zero.

Boundary conditions.- The boundary conditions on equation (2) are as follows:

At $\eta = 0$ (the pyrolysis interface), the heat conducted in is equal to the heat absorbed by the pyrolysis reaction

$$\frac{k}{\delta} \frac{\partial T}{\partial \eta} = \dot{m}_p \Delta h_p \quad (5)$$

where $\dot{m}_p$ is obtained from an Arrhenius-type equation

$$\dot{m}_p = A_i e^{-\frac{B_i}{T}}$$

The effect of the uncharred material on the ablative performance of the char layer can be roughly approximated by including the sensible heat absorption of this material in the heat of pyrolysis Δh_p.

At $\eta = 1$ (the char surface), the heat conducted in is equal to the net heat input to the surface

$$\frac{k}{\delta}\frac{\partial T}{\partial \eta} = q_s - \sigma\epsilon T^4 \tag{6}$$

where (see ref. 3)

$$q_s = q_C\left(1 - \frac{h_w}{h_e}\right)\left[1 - 0.6\,\frac{h_e}{q_C}\alpha_s\dot{m}_y + 0.084\left(\frac{h_e}{q_C}\alpha_s\dot{m}_y\right)^2\right] + \alpha q_R + \dot{m}_c\,\Delta h_c$$

The quadratic expression in $\dot{m}_y$ is a second-order approximation to a curve obtained from the boundary-layer program of reference 11 for air to air injection. The expression is valid for both blowing and suction at the wall (positive and negative $\dot{m}_y$). The mass loss rate of char at the surface $\dot{m}_c$ is obtained from an equation for first-order oxidation (see ref. 3) and is

$$\dot{m}_c = \frac{Kp_w C_e}{1 + \dfrac{Kp_w(h_e - h_w)}{\lambda q_{C,net}}} \tag{7}$$

where

$$K = A_s e^{-\frac{B_s}{T}}$$

and

$$q_{C,net} = q_C\left(1 - \frac{h_w}{h_e}\right)\left[1 - 0.6\,\frac{h_e}{q_C}\alpha_s\dot{m}_y + 0.084\left(\frac{h_e}{q_C}\alpha_s\dot{m}_y\right)^2\right]$$

At $x = 0$, and $x = L$, the temperature gradient is zero

$$\frac{DT}{\partial x} = \frac{\partial T}{\partial x} - A\,\frac{\partial T}{\partial \eta} = 0 \tag{8}$$

Although at $x = L$, this boundary condition is usually physically incorrect, it should be adequate especially if this boundary occurs outside the area where two-dimensional effects are significant.

Differential Equations for the Pressure Distribution

Governing pressure equation.- To obtain the governing differential equation for the pressure distribution in the char layer, it is assumed that the pressure distribution can be described by using Darcy's Law (ref. 12)

$$\vec{v} = -\frac{\kappa}{\mu}\nabla p \tag{9}$$

Multiplying both sides of equation (9) by ρ_g and assuming $\rho_g = \frac{pM}{R_o T}$ yields

$$\vec{\dot{m}} = -\frac{\kappa M}{2\mu R_o T} \nabla p^2 \tag{10}$$

Then by conservation of mass,

$$-\nabla \cdot \vec{\dot{m}} = \nabla \cdot \varphi \nabla p^2 = f \frac{D\rho_g}{\partial \tau} \tag{11}$$

where

$$\varphi = \frac{\kappa M}{2\mu R_o T} \tag{12}$$

and f is the porosity of the char layer.

By using the same development which was used for the temperature differential equation, the pressure equation (eq. (11)) becomes

$$\frac{\partial}{\partial x}\left(\frac{h_2}{h_1} \varphi \frac{\partial p^2}{\partial x}\right) - \frac{\partial}{\partial x}\left(\frac{h_2}{h_1} \varphi A \frac{\partial p^2}{\partial \eta}\right) - A \frac{\partial}{\partial \eta}\left(\frac{h_2}{h_1} \varphi \frac{\partial p^2}{\partial x}\right)$$

$$+ A \frac{\partial}{\partial \eta}\left(\frac{h_2}{h_1} \varphi A \frac{\partial p^2}{\partial \eta}\right) + \frac{1}{\delta^2} \frac{\partial}{\partial \eta}\left(h_1 h_2 \varphi \frac{\partial p^2}{\partial \eta}\right)$$

$$= h_1 h_2 f \left[\frac{\partial \rho_g}{\partial \tau} + \frac{\eta \dot{m}_c}{\delta \rho} \frac{\partial \rho_g}{\partial \eta} + \frac{(1 - \eta)\dot{m}_p}{(\rho' - \rho)\delta} \frac{\partial \rho_g}{\partial \eta}\right] \tag{13}$$

Initial conditions.- The initial conditions that must be specified are the pressure distribution and the body shape. The initial temperature distribution and mass loss rates that are required to solve the pressure equation (see eqs. (12) and (13)), are obtained from the solution of the temperature equation.

Boundary conditions.- The boundary conditions on equation (13) are as follows:

At $\eta = 0$ (the pyrolysis interface), the pressure gradient is proportional to the pyrolysis rate

$$\frac{\partial p^2}{\partial \eta} = -\frac{\dot{m}_p \delta}{\varphi} \tag{14}$$

At $\eta = 1$ (the char surface)

$$p^2(x) = p_e{}^2(x) \tag{15}$$

where p_e is specified as a function of location and time.

At $x = 0$, and $x = L$, the mass flux across the boundary is zero

$$\frac{Dp^2}{\partial x} = \frac{\partial p^2}{\partial x} - A\,\frac{\partial p^2}{\partial \eta} = \dot{m}_x = 0 \tag{16}$$

The previous discussion of the temperature boundary conditions at $x = L$ applies also to the pressure boundary conditions at this location.

Mass flow equations.- When the pressure distribution in the char layer has been determined from equations (13) to (16), the flow field $\dot{m}_x$ and $\dot{m}_y$ can be determined from equation (10). Thus,

$$\left.\begin{aligned} \dot{m}_x &= -\frac{\varphi}{h_1}\left(\frac{\partial p^2}{\partial x} - A\,\frac{\partial p^2}{\partial \eta}\right) \\ \dot{m}_y &= -\frac{\varphi}{\delta}\,\frac{\partial p^2}{\partial \eta} \end{aligned}\right\} \tag{17}$$

Coordinate Singularity

Equations (2) and (13) apply to the entire region of interest; however, a line of discontinuity (singularity) exists. An inspection of equation (A5) shows that at $x = 0$, that is, along the line of symmetry, the scale factor h_2 vanishes. This coordinate singularity can be eliminated by using proper approximations valid only near $x = 0$. The derivation of the differential equations which are used at the singularity is given in appendix B. The temperature equation at $x = 0$ is

$$2\,\frac{\partial}{\partial x}\left(\frac{k}{h_1}\,\frac{\partial T}{\partial x}\right) - 2\,\frac{\partial}{\partial x}\left(\frac{kA}{h_1}\,\frac{\partial T}{\partial \eta}\right) - 2A\,\frac{\partial}{\partial \eta}\left(\frac{k}{h_1}\,\frac{\partial T}{\partial x}\right) + 2A\,\frac{\partial}{\partial \eta}\left(\frac{kA}{h_1}\,\frac{\partial T}{\partial \eta}\right)$$

$$+ \frac{1}{\delta^2}\,\frac{\partial}{\partial \eta}\left(h_1 k\,\frac{\partial T}{\partial \eta}\right) + \frac{k}{R\delta}\,\frac{\partial T}{\partial \eta} - \frac{h_1 \dot{m}_y}{\delta}\,\frac{\partial}{\partial \eta}\left(\bar{c}_p T\right)$$

$$= h_1 \rho c_p\,\frac{\partial T}{\partial \tau} + \frac{h_1 c_p \eta \dot{m}_c}{\delta}\,\frac{\partial T}{\partial \eta} + \frac{h_1 \dot{m}_p \rho c_p (1 - \eta)}{\delta(\rho' - \rho)}\,\frac{\partial T}{\partial \eta} \tag{18}$$

The pressure equation at $x = 0$ is

$$2\frac{\partial}{\partial x}\left(\frac{\varphi}{h_1}\frac{\partial p^2}{\partial x}\right) - 2\frac{\partial}{\partial x}\left(\frac{\varphi A}{h_1}\frac{\partial p^2}{\partial \eta}\right) - 2A\frac{\partial}{\partial \eta}\left(\frac{\varphi}{h_1}\frac{\partial p^2}{\partial x}\right)$$

$$+ 2A\frac{\partial}{\partial \eta}\left(\frac{\varphi A}{h_1}\frac{\partial p^2}{\partial \eta}\right) + \frac{1}{\delta^2}\frac{\partial}{\partial \eta}\left(h_1\varphi\frac{\partial p^2}{\partial \eta}\right) + \frac{\varphi}{R\delta}\frac{\partial p^2}{\partial \eta}$$

$$= h_1 f\frac{\partial \rho_g}{\partial \tau} + \frac{h_1 f \eta \dot{m}_c}{\delta\rho}\frac{\partial \rho_g}{\partial \eta} + \frac{h_1 f(1-\eta)\dot{m}_p}{\delta(\rho' - \rho)}\frac{\partial \rho_g}{\partial \eta} \tag{19}$$

NUMERICAL PROCEDURES

Finite-Difference Equations

The differential equations were converted to finite-difference form through the use of the Taylor's series expansions. Forward, central, and backward differences were used. A summary of the finite-difference equations which are used in this analysis is given in appendix C.

Method of Solution

It was extremely difficult to find an acceptable method of solution for the finite-difference equations. Both standard matrix inversions and explicit methods were tried but were abandoned when the stable time interval became so small that 1 hour of compuputer time produced no significant progress.

The equations could not be solved entirely implicitly because of the nonlinear terms and the interdependence of the equations. Thus, an iterative procedure was required. The first choice of an implicit method was the alternating-direction method. (See ref. 13.) This method was not successful because, although the solution in the η-direction (columns) was reasonably accurate, the solution in the x-direction (rows) was not. It is postulated that the reason for this result is that the zero-slope boundary conditions at $x = 0$ and $x = L$ (eqs. (8) and (16)) do not serve to bound the solution. When only derivative boundary conditions are used, the shape of the curve can be determined, but the magnitude at any point cannot.

Other implicit methods of solution which were tried included a modified alternating-direction method (ref. 14) and a diagonal alternating-direction method (ref. 15). The method which was finally used to obtain solutions was to solve only the column equations

implicitly. The x-derivatives appear explicitly in the column equations. This approach is successful as long as the η-derivatives are considerably larger than the x-derivatives. When the lateral flow $\dot{m}_x$ becomes very large, some instability in the solution results. If the calculation continues to run, the instability generally subsides and does not appear to contribute significant errors in the final solution. In more severe cases, the solution diverges sufficiently to cause the program to stop or to make the solution meaningless. A method of solution which always remains stable was not found.

RESULTS AND DISCUSSION

The numerical analysis was compared with three simplified exact solutions to determine the accuracy of the finite-difference expressions. The exact solutions involve either the temperature equations or the pressure equations separately. The derivations of the exact solutions are given in appendix D. The complete numerical analysis was used to provide solutions for two body shapes subjected to a typical entry heating environment. Pronounced effects of the lateral flow of gases on the mass flow field within the char layer and the associated surface and pyrolysis interface recession rates are shown.

Comparisons With Exact Solutions

Three comparisons were made between the numerical analysis and exact solutions. The temperature equations are compared with an exact solution for a rectangular char layer undergoing quasi-steady-state ablation. The pressure equations are compared with two steady-state exact solutions, one for a rectangular char layer and one for a hemispherical section.

Quasi-steady-state temperature solution.- The comparison between the quasi-steady-temperature distribution obtained with the exact solution (eq. (D3)), and the distribution from the numerical analysis, is shown in table I. The input values used are shown, and the percent error at representative locations is given. The percent error values are calculated from the equation shown in the table. The maximum errors occur at the $x = 0$ locations and decrease as x increases. The maximum error of 0.277 percent is considered to be acceptable. The average error is 0.162 percent.

Pressure distribution for a rectangle.- The comparison between the pressure distribution for a rectangle obtained with the exact solution (eq. (D6)) and the distribution from the numerical solution is shown in table II. The input values used are shown and the percent error at various locations is given. The maximum errors occur at large values of x and small η-values. The largest error is 0.18 percent and the average error is 0.065 percent.

The errors in the mass-flow-rate components are shown in table III. The errors are an order of magnitude larger than the errors in the pressure distribution. The mass-

flow-rate components (eqs. (D7)) are obtained from derivatives (eqs. (17)), and it is very difficult to obtain accurate derivatives numerically. It appears that these errors are within the accuracy of the numerical method. Efforts to decrease the errors by including higher order terms in the derivatives were unsuccessful.

Spherical pressure distribution.- The comparison between the pressure distribution for a hemisphere obtained with the exact solution (eq. (D10)) and the distribution from the numerical solution is shown in table IV. The input values used are shown and the percent error at various locations is given. The largest error is 0.794 percent and the average error is 0.289 percent.

The errors in the mass-flow-rate components (eq. (D11)) are shown in table V. The errors are again an order of magnitude larger than the pressure errors.

Typical Calculated Results

Typical calculated results are given for two entry body shapes; these results were obtained by using the enthalpy, stagnation heating rate, and stagnation pressure histories shown in figure 4. These histories are typical of a ballistic entry from earth orbit.

The two body shapes used in the calculations are shown in figure 5. Figure 5(a) shows a hemispherically blunted cone shape and figure 5(b) shows a hemisphere-cone body. The part of each shape considered in the analysis lies between the $x = 0$ and $x = L$ lines. Beyond the $x = L$ line, the surface conditions become nearly constant with x. The material property values used in the calculations are given in table VI.

Hemispherically blunted cone.- The heating rate and pressure distributions around the blunt-faced body are shown in figure 6 as a function of distance along the reference surface. (See fig. 5(a).) Figure 6 shows a sharp pressure gradient at the first tangent point. (This point is the point where the large nose radius intersects the small corner radius.) Because of the large pressure drop around the corner, a low-pressure area exists in the vicinity of a high-pressure area. This condition can produce a large lateral flow effect because the gases within the char tend to flow laterally toward the low-pressure region rather than in the direction normal to the pyrolysis interface.

The effect of the lateral flow within the char layer is shown in figures 7 and 8. Figure 7 shows the mass flow, normal to the surface, at a point immediately preceding the sharp pressure drop. This station, in the analytical solution, is where the largest lateral flow effect is observed. A calculation with lateral flow and one in which lateral flow is not allowed $\left(\dot{m}_x = 0\right)$ are shown. In the early part of the trajectory, no lateral-flow effect is evident because the lateral-flow effect is dependent not only on the pressure gradient but also on the value of the pressure and on the char thickness. These latter two values are both small early in the trajectory.

As the char thickness and pressure increase later in the trajectory, lateral flow not only decreases the mass flow at the surface but actually produces an inflow of the boundary-layer gases into the char layer. The decrease in mass flow out through the surface decreases blocking of the convective heating. When the surface mass flow becomes negative, the convective heating rate becomes higher than it would be for an impermeable surface.

Figure 8 shows total surface and interface recession as a function of distance along the reference surface. Both the lateral-flow solution and the no-lateral-flow solution are shown. There is a very small difference in recession at the stagnation point $x = 0$. The lateral-flow effect is inversely proportional to the nose radius. Thus, although the effect is present, it is small because of the large hemispherical radius of the blunted cone. The differences in recession near the corner are significant. There is more recession at the corner than at the stagnation point for both cases because of the heating-rate peak. (See fig. 6.) However, the case with lateral flow shows considerably more recession. The increased surface recession is caused by increased oxidation which is due to the higher convective heating associated with reduced blocking and eventual inflow at the surface. The more significant increase in pyrolysis interface recession is caused mainly by the increased temperature gradients caused by the decrease in char cooling by the pyrolysis gases and the eventual influx of hot boundary-layer gas into the char layer.

Near $x = L$, the lateral flow case shows less recession than the no-lateral flow case because the gases that were flowing laterally through the char come out through the surface in this region of low pressure, increase the blocking of convective heating, and decrease the surface temperature.

The high recession rate near the corner has been observed experimentally on ablative heat shields of this shape. Previously, this large recession has been attributed to mechanical removal. The results presented here show that the lateral flow effect with its accompanying high oxidation rates can cause the observed shape change.

Hemisphere-cone.- The heating rate and pressure distributions on the hemisphere-cone body (fig. 5(b)) are shown in figure 9. Figure 10 shows the mass flow normal to the surface at the stagnation point ($x = 0$). When the char-layer thickness and pressure become large enough, the mass flow through the surface decreases and eventually becomes negative. This condition causes the increased recession shown in figure 11. Again the difference in recession is greater at the pyrolysis interface because the influx of hot boundary-layer gas has a greater effect on the internal temperature gradient than the increase in convective heating has on oxidation.

CRITERION FOR ASSESSING THE IMPORTANCE OF LATERAL FLOW

Since the analysis described in this paper is difficult to use, it is desirable to have a criterion which will indicate whether lateral flow should be considered or whether a one-dimensional ablation analysis is adequate. This criterion can be developed from the exact solution for the pressure distribution in a hemispherical char layer and a one-dimensional ablation analysis such as the analysis of reference 3. A lateral-flow parameter for a hemisphere can be obtained from appendix D. From appendix D (eq. (D12)), the mass flow at the surface is

$$\dot{m}_y = -2\varphi p_t{}^2\left(\cos 2\psi - \frac{1}{3}\right)\frac{\dfrac{R_{\psi,r}}{R_1{}^2} - \dfrac{R_1{}^3}{R_{\psi,r}^4}}{\left(\dfrac{R_2}{R_1}\right)^2 + \dfrac{2}{3}\left(\dfrac{R_1}{R_2}\right)^3} \tag{20}$$

The point on a hemisphere where lateral flow has the largest detrimental effect is at the stagnation point. At this point $\psi = 0^o$ and $R_{\psi,r} = R_2$. By assuming that the char thickness is small so that terms of order δ^2 can be neglected, equation (20) can be reduced to

$$\dot{m}_y = -\frac{4\varphi p_t{}^2\delta}{R_1{}^2} \tag{21}$$

If this mass flow rate is small compared with the pyrolysis rate of a one-dimensional stagnation-point analysis, then the lateral-flow effect should not be significant.

To determine at what value the mass flow of equation (21) can be considered small compared with the pyrolysis rate in a one-dimensional analysis, the calculations for the hemisphere-cone (fig. 5(b)) were evaluated. At 40 seconds the ratio of the mass flow of equation (21) to the one-dimensional pyrolysis rate is -0.001, at 50 seconds the ratio is -0.012, at 60 seconds the ratio is -0.145, and at 70 seconds the ratio is -0.65. An examination of figure 10 shows that the lateral-flow effect becomes important between 50 and 60 seconds. Therefore, it appears that if

$$\left|\frac{(\dot{m}_{y,t})_{2\text{-}D}}{(\dot{m}_p)_{1\text{-}D}}\right| < 0.1 \tag{22}$$

a one-dimensional analysis is probably sufficient.

Although this criterion was developed for a hemisphere with constant char thickness, it should be useful for most blunt bodies if the char thickness is small compared with the radius of curvature of the surface. For example, if the corner radius of the blunted-cone shape (fig. 5(a)) is used in equation (21), then equation (22) predicts that the lateral-flow effect becomes significant after 50 seconds. This result is consistent with the results shown in figure 7.

CONCLUDING REMARKS

Differential equations governing the temperature and pressure fields within an axisymmetric char layer were derived for assessing the effects of two-dimensional mass flow within the char layer. The equations were written in terms of general curvilinear coordinates, expanded into finite-difference form, and programed for numerical solution on a digital computer.

Numerical results compare favorably with exact solutions for simplified cases. Numerical solutions for the complete set of equations are shown for two body shapes subjected to a typical ballistic entry environment. Results show that including the effect of the lateral flow of gases within the char layer has a significant effect on the performance of the ablation material. In areas where the lateral flow effect is pronounced, blocking of the convective heating is reduced and the mass flow normal to the surface may even become negative. In these areas there is a significant increase in the surface temperature and in the surface and pyrolysis interface recession. The results shown through this analysis may explain some experimental ablation material recession data which could previously only be attributed to mechanical removal.

Langley Research Center,
National Aeronautics and Space Administration,
Hampton, Va., July 28, 1972.

APPENDIX A

DEVELOPMENT OF GOVERNING DIFFERENTIAL EQUATION

This appendix describes the derivation of the differential equation that will be converted into finite-difference form.

The governing vector equation for the temperature distribution in the char layer is

$$\underbrace{\nabla \cdot k\nabla T}_{\text{Heat conducted}} - \underbrace{\nabla \cdot \left(\vec{\dot{m}}\bar{c}_p T\right)}_{\text{Heat absorbed by pyrolysis gases}} = \underbrace{\frac{\partial}{\partial \tau}\left[\left(\rho c_p + \rho_g \bar{c}_p\right)T\right]}_{\text{Heat stored}} \tag{A1}$$

By assuming that the density of the char layer is constant, that the specific heats of both the char and the pyrolysis gases are functions of temperature only, and that $\rho_g << \rho$, the right-hand side of equation (A1) can be written as

$$\frac{\partial}{\partial \tau}\left[\left(\rho c_p + \rho_g \bar{c}_p\right)T\right] \approx \rho c_p \frac{\partial T}{\partial \tau} + \bar{c}_p T \frac{\partial \rho_g}{\partial \tau}$$

Equation (A1) can now be written as

$$\nabla \cdot k\nabla T - \vec{\dot{m}} \cdot \nabla\left(\bar{c}_p T\right) = \rho c_p \frac{\partial T}{\partial \tau} + \bar{c}_p T\left(\frac{\partial \rho_g}{\partial \tau} + \nabla \cdot \dot{m}\right)$$

Since the quantity within the parentheses in the last term is the continuity equation, the last term is equal to zero. Therefore equation (A1) becomes

$$\nabla \cdot k\nabla T - \vec{\dot{m}} \cdot \nabla\left(\bar{c}_p T\right) = \rho c_p \frac{\partial T}{\partial \tau} \tag{A2}$$

Because the surface and the pyrolysis interface locations are changing with time, it is convenient to make the transformation

$$\eta = \frac{y - y_p}{\delta}$$

where

y_p thickness of uncharred material

δ thickness of char layer

With this transformation, the η-coordinate always goes from 0 to 1 through the char thickness δ. The result is a moving coordinate system in the y-direction.

Because δ and y_p are functions of x, η is also. Therefore, total derivatives rather than partial derivatives must be used in the x-direction. This total derivative can be written (ref. 16) as

$$\frac{D(\ )}{\partial x} = \frac{\partial}{\partial x} + \frac{\partial \eta}{\partial x}\frac{\partial}{\partial \eta} = \frac{\partial}{\partial x} - A\frac{\partial}{\partial \eta}$$

where

$$A = \frac{\partial \eta}{\partial x} = \frac{1}{\delta}\left(\eta\frac{\partial \delta}{\partial x} + \frac{\partial y_p}{\partial x}\right)$$

Total derivatives with respect to time must also be used to give

$$\frac{DT}{\partial \tau} = \frac{\partial T}{\partial \tau} + \frac{\partial \eta}{\partial \tau}\frac{\partial T}{\partial \eta}$$

and since

$$\frac{\partial \eta}{\partial \tau} = \frac{\partial \eta}{\partial \delta}\frac{\partial \delta}{\partial \tau} + \frac{\partial \eta}{\partial y_p}\frac{\partial y_p}{\partial \tau}$$

then

$$\frac{DT}{\partial \tau} = \frac{\partial T}{\partial \tau} + \left(\frac{\partial \eta}{\partial \delta}\frac{\partial \delta}{\partial \tau} + \frac{\partial \eta}{\partial y_p}\frac{\partial y_p}{\partial \tau}\right)\frac{\partial T}{\partial \eta} \tag{A3}$$

The change in δ is

$$\delta - \delta_o = -\int \frac{\dot{m}_c}{\rho}\,d\tau + \int \frac{\dot{m}_p}{\rho' - \rho}\,d\tau$$

where (see fig. 2)

$\dot{m}_c$ mass loss rate due to char removal at surface

$\dot{m}_p$ mass flow rate at pyrolysis interface due to pyrolysis reactions

From the preceding equation,

$$\frac{\partial \delta}{\partial \tau} = -\frac{\dot{m}_c}{\rho} + \frac{\dot{m}_p}{\rho' - \rho}$$

The change in y_p is

$$y_p - y_{p,o} = -\int \frac{\dot{m}_p}{\rho' - \rho} d\tau$$

Thus

$$\frac{\partial y_p}{\partial \tau} = -\frac{\dot{m}_p}{\rho' - \rho}$$

Then, since

$$\frac{\partial \eta}{\partial \delta} = -\frac{\eta}{\delta}$$

$$\frac{\partial \eta}{\partial y_p} = -\frac{1}{\delta}$$

equation (A3) becomes

$$\frac{DT}{d\tau} = \frac{\partial T}{\partial \tau} + \left[\frac{\eta \dot{m}_c}{\delta \rho} + \frac{(1 - \eta)\dot{m}_p}{(\rho' - \rho)\delta}\right]\frac{\partial T}{\partial \eta} \tag{A4}$$

The equation is transformed to a curvilinear coordinate system through the use of scale factors. (See ref. 10.) The differential arc length ds in the curvilinear coordinate system shown in figure 3 is

$$(ds)^2 = h_1^2(dx)^2 + h_2^2(d\varphi)^2 + h_3^2(dy)^2$$

where the scale factors are

$$\left.\begin{aligned} h_1 &= 1 + \frac{y}{R} \\ h_2 &= R_s + y \cos \beta \\ h_3 &= 1 \end{aligned}\right\} \tag{A5}$$

The curvilinear coordinate system should conveniently describe any axisymmetric body geometry of interest. However, if the Cartesian coordinate system is required, care must be taken to make all scale factors equal one.

To make the analysis more tractable, it is assumed that no temperature gradients exist in the θ-direction. This assumption limits the analysis to axisymmetric shapes and flow fields.

Through the use of the preceding development, the final form of the differential temperature equation is obtained by combining equations (A2), (A4), and (A5) and is

$$\frac{\partial}{\partial x}\left(\frac{h_2}{h_1} k \frac{\partial T}{\partial x}\right) - \frac{\partial}{\partial x}\left(\frac{h_2}{h_1} kA \frac{\partial T}{\partial \eta}\right) - A \frac{\partial}{\partial \eta}\left(\frac{h_2}{h_1} k \frac{\partial T}{\partial x}\right) + \dot{A} \frac{\partial}{\partial \eta}\left(\frac{h_2}{h_1} kA \frac{\partial T}{\partial \eta}\right)$$

$$+ \frac{1}{\delta^2} \frac{\partial}{\partial \eta}\left(h_1 h_2 k \frac{\partial T}{\partial \eta}\right) - h_2 \dot{m}_x \frac{\partial}{\partial x}\left(\bar{c}_p T\right) + h_2 A \dot{m}_x \frac{\partial}{\partial \eta}\left(\bar{c}_p T\right) - \frac{h_1 h_2 \dot{m}_y}{\delta} \frac{\partial}{\partial \eta}\left(\bar{c}_p T\right)$$

$$= h_1 h_2 \rho c_p \frac{\partial T}{\partial \tau} + \frac{h_1 h_2 c_p \eta \dot{m}_c}{\delta} \frac{\partial T}{\partial \eta} + \frac{h_1 h_2 (1 - \eta) \dot{m}_p \rho c_p}{(\rho' - \rho)\delta} \frac{\partial T}{\partial \eta} \tag{A6}$$

The procedure used to develop the pressure equation is very similar and will not be given. The final form of the differential-pressure equation is given by equation (13).

APPENDIX B

DERIVATION OF THE DIFFERENTIAL EQUATIONS AT THE COORDINATE SINGULARITY

In this appendix, only the derivation of the temperature equation at $x = 0$ will be given. The derivation of the pressure equation at the coordinate singularity is similar.

The derivation of the temperature equation when $h_2 = 0$ is initiated by determining the behavior of h_2 as $x \to 0$. As $x \to 0$, $R_s \to x$ and $\cos \beta \to \frac{R_s}{R} \to \frac{x}{R}$. Therefore,

$$(h_2)_{x \to 0} = x\left(1 + \frac{y}{R}\right) \tag{B1}$$

$$\left(\frac{\partial h_2}{\partial x}\right)_{x \to 0} = 1 + \frac{y}{R} = h_1 \tag{B2}$$

and

$$\left(\frac{\partial h_2}{\partial y}\right)_{x \to 0} = \frac{x}{R} \tag{B3}$$

The temperature equation is evaluated at the coordinate singularity by using equation (A2) with the scale factors included. Equation (A2) can be written as

$$\frac{1}{h_1 h_2}\left[\frac{\partial}{\partial x}\left(\frac{h_2}{h_1} k \frac{\partial T}{\partial x}\right) + \frac{\partial}{\partial y}\left(h_1 h_2 k \frac{\partial T}{\partial y}\right)\right] - \frac{\dot{m}_x}{h_1}\frac{\partial}{\partial x}\left(\bar{c}_p T\right) - \dot{m}_y \frac{\partial}{\partial y}\left(\bar{c}_p T\right) = \rho c_p \frac{\partial T}{\partial \tau} \tag{B4}$$

The first two terms of equation (B4) must be modified because of the coordinate singularity. By using equations (B1), (B2), and (B3) and L'Hospital's rule, the first term can be evaluated as follows:

$$\frac{1}{h_1 h_2}\frac{\partial}{\partial x}\left(\frac{h_2}{h_1} k \frac{\partial T}{\partial x}\right) = \frac{1}{h_1}\frac{\partial}{\partial x}\left(\frac{k}{h_1}\frac{\partial T}{\partial x}\right) + \frac{k}{h_1^2 h_2}\frac{\partial T}{\partial x}\frac{\partial h_2}{\partial x} = \frac{1}{h_1}\frac{\partial}{\partial x}\left(\frac{k}{h_1}\frac{\partial T}{\partial x}\right) + \frac{k}{h_1 h_2}\frac{\partial T}{\partial x}$$

Then, since $\frac{\partial T}{\partial x} = 0$ at $x = 0$,

$$\frac{k}{h_1 h_2}\frac{\partial T}{\partial x} = \lim_{x \to 0} \frac{\frac{\partial}{\partial x}\left(\frac{k}{h_1}\frac{\partial T}{\partial x}\right)}{\partial h_2/\partial x} = \frac{1}{h_1}\frac{\partial}{\partial x}\left(\frac{k}{h_1}\frac{\partial T}{\partial x}\right)$$

Therefore,

$$\left[\frac{1}{h_1 h_2}\frac{\partial}{\partial x}\left(\frac{h_2}{h_1} k \frac{\partial T}{\partial x}\right)\right]_{x \to 0} = \frac{2}{h_1}\frac{\partial}{\partial x}\left(\frac{k}{h_1}\frac{\partial T}{\partial x}\right) \tag{B5}$$

A similar procedure is used to evaluate the second term

$$\frac{1}{h_1 h_2}\frac{\partial}{\partial y}\left(h_1 h_2 k \frac{\partial T}{\partial y}\right) = \frac{1}{h_1}\frac{\partial}{\partial y}\left(h_1 k \frac{\partial T}{\partial y}\right) + \frac{k}{h_2}\frac{\partial T}{\partial y}\frac{\partial h_2}{\partial y} = \frac{1}{h_1}\frac{\partial}{\partial y}\left(h_1 k \frac{\partial T}{\partial y}\right) + \frac{k}{x\left(1 + \frac{y}{R}\right)}\frac{\partial T}{\partial y}\frac{x}{R}$$

Therefore,

$$\left[\frac{1}{h_1 h_2}\frac{\partial}{\partial y}\left(h_1 h_2 k \frac{\partial T}{\partial y}\right)\right]_{x \to 0} = \frac{1}{h_1}\frac{\partial}{\partial y}\left(h_1 k \frac{\partial T}{\partial y}\right) + \frac{k}{h_1 R}\frac{\partial T}{\partial y} \tag{B6}$$

The differential equation for the temperature distribution at the coordinate singularity can now be given. By using equations (B5) and (B6) in equation (B4) and including the transformation of equation (3), the temperature equation at $x = 0$ is

$$2\frac{\partial}{\partial x}\left(\frac{k}{h_1}\frac{\partial T}{\partial x}\right) - 2\frac{\partial}{\partial x}\left(\frac{kA}{h_1}\frac{\partial T}{\partial \eta}\right) - 2A\frac{\partial}{\partial \eta}\left(\frac{k}{h_1}\frac{\partial T}{\partial x}\right) + 2A\frac{\partial}{\partial \eta}\left(\frac{kA}{h_1}\frac{\partial T}{\partial \eta}\right)$$

$$+ \frac{1}{\delta^2}\frac{\partial}{\partial \eta}\left(h_1 k \frac{\partial T}{\partial \eta}\right) + \frac{k}{R\delta}\frac{\partial T}{\partial \eta} - h_1\frac{\dot{m}_y}{\delta}\frac{\partial}{\partial \eta}\left(\bar{c}_p T\right)$$

$$= h_1 \rho c_p \frac{\partial T}{\partial \tau} + \frac{h_1 c_p \eta \dot{m}_c}{\delta}\frac{\partial T}{\partial \eta} + \frac{h_1(1 - \eta)\dot{m}_p \rho c_p}{(\rho' - \rho)\delta}\frac{\partial T}{\partial \eta} \tag{B7}$$

APPENDIX C

FINITE-DIFFERENCE EQUATIONS

Temperature Equations

The finite-difference temperature equations are as follows: (The m subscript corresponds to the η-coordinate, $m = 1$ being $\eta = 0$ and $m = s$ being $\eta = 1$. The n subscript corresponds to the x coordinate, $n = 1$ being $x = 0$ and $n = L$ being $x = L$.) For $1 < m < s$, $1 < n < L$, the equation is

$$\frac{\left(\frac{h_2}{h_1}k\right)_{m,n+\frac{1}{2}}T_{m,n+1} - \left[\left(\frac{h_2}{h_1}k\right)_{m,n+\frac{1}{2}} + \left(\frac{h_2}{h_1}k\right)_{m,n-\frac{1}{2}}\right]T_{m,n} + \left(\frac{h_2}{h_1}k\right)_{m,n-\frac{1}{2}}T_{m,n-1}}{\Delta x^2}$$

$$- \frac{\left(\frac{h_2}{h_1}kA\right)_{m,n+1}\left(T_{m+1,n+1} - T_{m-1,n+1}\right) - \left(\frac{h_2}{h_1}kA\right)_{m,n-1}\left(T_{m+1,n-1} - T_{m-1,n-1}\right)}{4\,\Delta\eta\,\Delta x}$$

$$- A_{m,n}\left[\frac{\left(\frac{h_2}{h_1}k\right)_{m+1,n}\left(T_{m+1,n+1} - T_{m+1,n-1}\right) - \left(\frac{h_2}{h_1}k\right)_{m-1,n}\left(T_{m-1,n+1} - T_{m-1,n-1}\right)}{4\,\Delta\eta\,\Delta x}\right]$$

$$+ A_{m,n}\left\{\frac{\left(\frac{h_2}{h_1}kA\right)_{m+\frac{1}{2},n}T_{m+1,n}}{\Delta\eta^2} - \frac{\left[\left(\frac{h_2}{h_1}kA\right)_{m+\frac{1}{2},n} + \left(\frac{h_2}{h_1}kA\right)_{m-\frac{1}{2},n}\right]T_{m,n}}{\Delta\eta^2} + \frac{\left(\frac{h_2}{h_1}kA\right)_{m-\frac{1}{2},n}T_{m-1,n}}{\Delta\eta^2}\right\}$$

$$+ \frac{1}{\delta_n^2}\left\{\frac{\left(h_1h_2k\right)_{m+\frac{1}{2},n}T_{m+1,n} - \left[\left(h_1h_2k\right)_{m+\frac{1}{2},n} + \left(h_1h_2k\right)_{m-\frac{1}{2},n}\right]T_{m,n}}{\Delta\eta^2} + \frac{\left(h_1h_2k\right)_{m-\frac{1}{2},n}T_{m-1,n}}{\Delta\eta^2}\right\}$$

$$- \left(h_2\dot{m}_x\right)_{m,n}\frac{\left(\bar{c}_pT\right)_{m,n+1} - \left(\bar{c}_pT\right)_{m,n-1}}{2\,\Delta x} + \left(h_2A\dot{m}_x\right)_{m,n}\frac{\left(\bar{c}_pT\right)_{m+1,n} - \left(\bar{c}_pT\right)_{m-1,n}}{2\,\Delta\eta}$$

$$- \frac{\left(h_1h_2\dot{m}_y\right)_{m,n}}{\delta_n}\frac{\left(\bar{c}_pT\right)_{m+1,n} - \left(\bar{c}_pT\right)_{m-1,n}}{2\,\Delta\eta} - \left(\frac{h_1h_2c_p\eta\dot{m}_c}{\delta}\right)_{m,n}\frac{T_{m+1,n} - T_{m-1,n}}{2\,\Delta\eta}$$

$$- \left[\frac{(1-\eta)}{(\rho' - \rho)}\frac{\dot{m}_p\rho h_1h_2c_p}{\delta}\right]_{m,n}\frac{T_{m+1,n} - T_{m-1,n}}{2\,\Delta\eta} - \left(h_1h_2\rho c_p\right)_{m,n}\frac{T_{m,n} - \left(T_o\right)_{m,n}}{\Delta\tau} = 0 \qquad \text{(C1)}$$

For $m = 1$, $1 < n < L$, the equation is

$$\frac{\left(\frac{h_2}{h_1}k\right)_{1,n+\frac{1}{2}} T_{1,n+1} - \left[\left(\frac{h_2}{h_1}k\right)_{1,n+\frac{1}{2}} + \left(\frac{h_2}{h_1}k\right)_{1,n-\frac{1}{2}}\right] T_{1,n} + \left(\frac{h_2}{h_1}k\right)_{1,n-\frac{1}{2}} T_{1,n-1}}{\Delta x^2}$$

$$- \frac{\left(\frac{h_2}{h_1} A\delta\dot{m}_p \Delta h_p\right)_{1,n+\frac{1}{2}} - \left(\frac{h_2}{h_1} A\delta\dot{m}_p \Delta h_p\right)_{1,n-\frac{1}{2}}}{\Delta x}$$

$$- A_{1,n}\left[\frac{\left(\frac{h_2}{h_1}k\right)_{2,n}\left(T_{2,n+1} - T_{2,n-1}\right)}{\Delta\eta\,\Delta x} - \frac{\left(\frac{h_2}{h_1}k\right)_{3,n}\left(T_{3,n+1} - T_{3,n-1}\right)}{4\,\Delta\eta\,\Delta x} - \frac{3\left(\frac{h_2}{h_1}k\right)_{1,n}\left(T_{1,n+1} - T_{1,n-1}\right)}{4\,\Delta\eta\,\Delta x}\right]$$

$$+ A_{1,n}\left[\frac{3\left(\frac{h_2}{h_1}kA\right)_{\frac{3}{2},n}\left(T_{2,n} - T_{1,n}\right)}{\Delta\eta^2} - \frac{\left(\frac{h_2}{h_1}kA\right)_{\frac{5}{2},n}\left(T_{3,n} - T_{2,n}\right)}{3\,\Delta\eta^2} - \frac{8}{3\,\Delta\eta}\left(\frac{h_2}{h_1} A\delta\dot{m}_p \Delta h_p\right)_{1,n}\right]$$

$$+ \frac{1}{\delta^2}\left[3\left(h_1h_2k\right)_{\frac{3}{2},n}\frac{\left(T_{2,n} - T_{1,n}\right)}{\Delta\eta^2} - \left(h_1h_2k\right)_{\frac{5}{2},n}\frac{\left(T_{3,n} - T_{2,n}\right)}{3\,\Delta\eta^2} - \frac{8}{3\,\Delta\eta}\left(h_1h_2\delta\dot{m}_p \Delta h_p\right)_{1,n}\right]$$

$$- \left(h_2\dot{m}_x\right)_{1,n}\frac{\left(\bar{c}_pT\right)_{1,n+1} - \left(\bar{c}_pT\right)_{1,n-1}}{2\,\Delta x} + \left(h_2A\dot{m}_x\right)_{1,n}\frac{4\left(\bar{c}_pT\right)_{2,n} - \left(\bar{c}_pT\right)_{3,n} - 3\left(\bar{c}_pT\right)_{1,n}}{2\,\Delta\eta}$$

$$- \frac{\left(h_1h_2\dot{m}_y\right)_{1,n}}{\delta_n}\frac{4\left(\bar{c}_pT\right)_{2,n} - \left(\bar{c}_pT\right)_{3,n} - 3\left(\bar{c}_pT\right)_{1,n}}{2\,\Delta\eta} - \left[\frac{h_1h_2\rho c_p\dot{m}_p}{(\rho' - \rho)\delta}\right]_{1,n}\frac{4T_{2,n} - T_{3,n} - 3T_{1,n}}{2\,\Delta\eta}$$

$$- \left(h_1h_2\rho c_p\right)_{1,n}\frac{T_{1,n} - \left(T_o\right)_{1,n}}{\Delta\tau} = 0 \qquad \text{(C2)}$$

For $m = s$, $1 < n < L$, the equation is

$$\frac{\left(\frac{h_2}{h_1}k\right)_{s,n+\frac{1}{2}} T_{s,n+1} - \left[\left(\frac{h_2}{h_1}k\right)_{s,n+\frac{1}{2}} + \left(\frac{h_2}{h_1}k\right)_{s,n-\frac{1}{2}}\right] T_{s,n} + \left(\frac{h_2}{h_1}k\right)_{s,n-\frac{1}{2}} T_{s,n-1}}{\Delta x^2}$$

$$- \frac{\left[\frac{h_2}{h_1}\delta A\left(q_t - \sigma\epsilon T^4\right)\right]_{s,n+1} - \left[\frac{h_2}{h_1}\delta A\left(q_s - \sigma\epsilon T^4\right)\right]_{s,n-1}}{2\,\Delta x}$$

$$- A_{s,n}\left[\frac{3\left(\frac{h_2}{h_1}k\right)_{s,n}\left(T_{s,n+1} - T_{s,n-1}\right)}{4\,\Delta\eta\,\Delta x} + \frac{\left(\frac{h_2}{h_1}k\right)_{s-2,n}\left(T_{s-2,n+1} - T_{s-2,n-1}\right)}{4\,\Delta\eta\,\Delta x} - \frac{\left(\frac{h_2}{h_1}k\right)_{s-1,n}\left(T_{s-1,n+1} - T_{s-1,n-1}\right)}{\Delta\eta\,\Delta x}\right]$$

$$+ A_{s,n}\left\{\frac{\left(\frac{h_2}{h_1}kA\right)_{s-\frac{3}{2},n}\left(T_{s-1,n} - T_{s-2,n}\right)}{3\,\Delta\eta^2} - \frac{3\left(\frac{h_2}{h_1}kA\right)_{s-\frac{1}{2},n}\left(T_{s,n} - T_{s-1,n}\right)}{\Delta\eta^2} + \frac{8}{3\,\Delta\eta}\left[\frac{h_2}{h_1}A\delta\left(q_t - \sigma\epsilon T^4\right)\right]_{s,n}\right\}$$

$$+ \frac{1}{\delta_n{}^2}\left\{\frac{\left(h_1h_2k\right)_{s-\frac{3}{2},n}\left(T_{s-1,n} - T_{s-2,n}\right)}{3\,\Delta\eta^2} - \frac{3\left(h_1h_2k\right)_{s-\frac{1}{2},n}\left(T_{s,n} - T_{s-1,n}\right)}{\Delta\eta^2} + \frac{8}{3\,\Delta\eta}\left[h_1h_2\delta\left(q_t - \sigma\epsilon T^4\right)\right]_{s,n}\right\}$$

$$- \left(h_2\dot{m}_x\right)_{s,n}\frac{\left(\bar{c}_pT\right)_{s,n+1} - \left(\bar{c}_pT\right)_{s,n-1}}{2\,\Delta x} + \left(h_2A\dot{m}_x\right)_{s,n}\frac{\left(\bar{c}_pT\right)_{s-2,n} + 3\left(\bar{c}_pT\right)_{s,n} - 4\left(\bar{c}_pT\right)_{s-1,n}}{2\,\Delta\eta}$$

$$- \frac{\left(h_1h_2\dot{m}_y\right)_{s,n}}{\delta_n}\frac{\left(\bar{c}_pT\right)_{s-2,n} + 3\left(\bar{c}_pT\right)_{s,n} - 4\left(\bar{c}_pT\right)_{s-1,n}}{2\,\Delta\eta} - \frac{\left(h_1h_2c_p\dot{m}_c\right)_{s,n}}{\delta_n}\frac{3T_{s,n} + T_{s-2,n} - 4T_{s-1,n}}{2\,\Delta\eta}$$

$$- \left(h_1h_2\rho c_p\right)_{s,n}\frac{T_{s,n} - \left(T_o\right)_{s,n}}{\Delta\tau} = 0 \qquad \text{(C3)}$$

For $1 < m < s$, $n = 1$, the equation is

$$\frac{6\left(\frac{k}{h_1}\right)_{m,\frac{3}{2}}\left(T_{m,2} - T_{m,1}\right)}{\Delta x^2} - \frac{2\left(\frac{k}{h_1}\right)_{m,\frac{5}{2}}\left(T_{m,3} - T_{m,2}\right)}{3\,\Delta x^2}$$

$$- \frac{3\left(\frac{kA}{h_1}\right)_{m,\frac{3}{2}}\left[\left(T_{m+1,1} - T_{m-1,1}\right) + \left(T_{m+1,2} - T_{m-1,2}\right)\right]}{2\,\Delta\eta\,\Delta x}$$

$$+ \frac{\left(\frac{kA}{h_1}\right)_{m,\frac{5}{2}}\left[\left(T_{m+1,2} - T_{m-1,2}\right) + \left(T_{m+1,3} - T_{m-1,3}\right)\right]}{6\,\Delta x\,\Delta\eta}$$

$$+ \frac{1}{\delta_1^2}\left\{\frac{\left(h_1k\right)_{m+\frac{1}{2},1}T_{m+1,1}}{\Delta\eta^2} - \frac{\left[\left(h_1k\right)_{m+\frac{1}{2},1} + \left(h_1k\right)_{m-\frac{1}{2},1}\right]T_{m,1}}{\Delta\eta^2} + \frac{\left(h_1k\right)_{m-\frac{1}{2},1}T_{m-1,1}}{\Delta\eta^2}\right\}$$

$$+ \left(\frac{k}{R,\delta}\right)_{m,1}\frac{T_{m+1,1} - T_{m-1,1}}{2\,\Delta\eta} - \frac{\left(h_1\dot{m}_y\right)_{m,1}}{\delta_1}\frac{\left(\bar{c}_pT\right)_{m+1,1} - \left(\bar{c}_pT\right)_{m-1,1}}{2\,\Delta\eta}$$

$$- \left(\frac{h_1c_p\eta\dot{m}_c}{\delta}\right)_{m,1}\frac{T_{m+1,1} - T_{m-1,1}}{2\,\Delta\eta} - \left[\frac{(1-\eta)h_1\dot{m}_p\rho c_p}{(\rho' - \rho)\delta}\right]_{m,1}\frac{T_{m+1,1} - T_{m-1,1}}{2\,\Delta\eta}$$

$$- \left(h_1\rho c_p\right)_{m,1}\frac{T_{m,1} - \left(T_o\right)_{m,1}}{\Delta\tau} = 0 \qquad \text{(C4)}$$

For $1 < m < s$, $n = L$, the equation is

$$\frac{\left(\frac{h_2}{h_1}k\right)_{m,L-\frac{3}{2}}\left(T_{m,L-1} - T_{m,L-2}\right)}{3\,\Delta x^2} - \frac{3\left(\frac{h_2}{h_1}k\right)_{m,L-\frac{1}{2}}\left(T_{m,L} - T_{m,L-1}\right)}{\Delta x^2}$$

$$+ \frac{3\left(\frac{h_2}{h_1}kA\right)_{m,L-\frac{1}{2}}\left[\left(T_{m+1,L} - T_{m-1,L}\right) + \left(T_{m+1,L-1} - T_{m-1,L-1}\right)\right]}{4\,\Delta\eta\,\Delta x}$$

$$- \frac{\left(\frac{h_2}{h_1}kA\right)_{m,L-\frac{3}{2}}\left[\left(T_{m+1,L-1} - T_{m-1,L-1}\right) + \left(T_{m+1,L-2} - T_{m-1,L-2}\right)\right]}{12\,\Delta\eta\,\Delta x}$$

$$+ \frac{1}{\delta_L{}^2}\left\{\frac{\left(h_1h_2k\right)_{m+\frac{1}{2},L}T_{m+1,L}}{\Delta\eta^2} - \frac{\left[\left(h_1h_2k\right)_{m+\frac{1}{2},L} + \left(h_1h_2k\right)_{m-\frac{1}{2},L}\right]T_{m,L}}{\Delta\eta^2}\right.$$

$$\left. + \frac{\left(h_1h_2k\right)_{m-\frac{1}{2},L}T_{m-1,L}}{\Delta\eta^2}\right\} - \frac{\left(h_1h_2\dot{m}_y\right)_{m,L}}{\delta_L}\frac{\left(\bar{c}_pT\right)_{m+1,L} - \left(\bar{c}_pT\right)_{m-1,L}}{2\Delta\eta}$$

$$- \left(\frac{h_1h_2c_p\eta\dot{m}_c}{\delta}\right)_{m,L}\frac{T_{m+1,L} - T_{m-1,L}}{2\,\Delta\eta}$$

$$- \left(\frac{1-\eta}{\rho' - \rho}\frac{\dot{m}_p\rho c_ph_1h_2}{\delta}\right)_{m,L}\frac{T_{m+1,L} - T_{m-1,L}}{2\,\Delta\eta}$$

$$- \left(h_1h_2\rho c_p\right)_{m,L}\frac{T_{m,L} - \left(T_o\right)_{m,L}}{\Delta\tau} = 0 \qquad \text{(C5)}$$

For $m = 1$, $n = 1$, the equation is

$$\frac{6\left(\frac{k}{h_1}\right)_{1,\frac{3}{2}}\left(T_{1,2} - T_{1,1}\right)}{\Delta x^2} - \frac{2\left(\frac{k}{h_1}\right)_{1,\frac{5}{2}}\left(T_{1,3} - T_{1,2}\right)}{3\,\Delta x^2}$$

$$- \frac{3\left(\frac{A}{h_1}\right)_{1,\frac{3}{2}}\left[\left(\delta\dot{m}_p\,\Delta h_p\right)_{1,1} + \left(\delta\dot{m}_p\,\Delta h_p\right)_{1,2}\right]}{\Delta x}$$

$$+ \frac{\left(\frac{A}{h_1}\right)_{1,\frac{5}{2}}\left[\left(\delta\dot{m}_p\,\Delta h_p\right)_{1,2} + \left(\delta\dot{m}_p\,\Delta h_p\right)_{1,3}\right]}{3\,\Delta x}$$

$$+ \frac{1}{\delta_1^2}\left[\frac{3\left(h_1k\right)_{\frac{3}{2},1}\left(T_{2,1} - T_{1,1}\right)}{\Delta\eta^2} - \frac{\left(h_1k\right)_{\frac{5}{2},1}\left(T_{3,1} - T_{2,1}\right)}{3\,\Delta\eta^2} - \frac{8}{3\,\Delta\eta}\left(h_1\delta\dot{m}_p\,\Delta h_p\right)_{1,1}\right]$$

$$+ \left(\frac{m_p\,\Delta h_p}{R}\right)_{1,1} - \frac{\left(h_1\dot{m}_y\right)_{1,1}}{\delta_1}\,\frac{4\left(\bar{c}_pT\right)_{2,1} - \left(\bar{c}_pT\right)_{3,1} - 3\left(\bar{c}_pT\right)_{1,1}}{2\,\Delta\eta}$$

$$- \left[\frac{\dot{m}_p\rho c_p}{(\rho' - \rho)\delta}\right]_{1,1}\,\frac{4T_{2,1} - T_{3,1} - 3T_{1,1}}{2\,\Delta\eta}$$

$$- \left(h_1\rho c_p\right)_{1,1}\,\frac{T_{1,1} - \left(T_o\right)_{1,1}}{\Delta\tau} = 0 \qquad \text{(C6)}$$

For $m = s$, $n = 1$, the equation is

$$\frac{6\left(\frac{k}{h_1}\right)_{s,\frac{3}{2}}\left(T_{s,2} - T_{s,1}\right)}{\Delta x^2} - \frac{2\left(\frac{k}{h_1}\right)_{1,\frac{5}{2}}\left(T_{s,3} - T_{s,2}\right)}{3\,\Delta x^2}$$

$$- \frac{3\left(\frac{A}{h_1}\right)_{1,\frac{3}{2}}\left[\delta_1\left(q_t - \sigma\epsilon T^4\right)_{s,1} + \delta_2\left(q_s - \sigma\epsilon T^4\right)_{s,2}\right]}{\Delta x}$$

$$+ \frac{\left(\frac{A}{h_1}\right)_{1,\frac{5}{2}}\left[\delta_2\left(q_t - \sigma\epsilon T^4\right)_{s,2} + \delta_3\left(q_t - \sigma\epsilon T^4\right)_{s,3}\right]}{3\,\Delta x}$$

$$+ \frac{1}{\delta_1{}^2}\left[\frac{\left(h_1 k\right)_{s-\frac{3}{2},1}\left(T_{s-2,1} - T_{s-3,1}\right)}{3\,\Delta\eta^2} - \frac{3\left(h_1 k\right)_{s-\frac{1}{2},1}\left(T_{s,1} - T_{s-1,1}\right)}{\Delta\eta^2} + \frac{8}{3\,\Delta\eta}\left(h_1\delta\right)_{s,1}\left(q_t - \sigma\epsilon T^4\right)_{s,1}\right]$$

$$+ \left(\frac{q_t - \sigma\epsilon T^4}{R}\right)_{s,1} - \frac{\left(h_1\dot{m}_y\right)_{s,1}}{\delta_1}\,\frac{\left(\bar{c}_p T\right)_{s-2,1} - 4\left(\bar{c}_p T\right)_{s-1,1} + 3\left(\bar{c}_p T\right)_{s,1}}{2\,\Delta\eta}$$

$$- \left(\frac{h_1 c_p \dot{m}_c}{\delta}\right)_{s,1}\,\frac{3T_{s,1} - 4T_{s-1,1} + T_{s-2,1}}{2\,\Delta\eta}$$

$$- \left(h_1\rho c_p\right)_{s,1}\,\frac{T_{s,1} - \left(T_o\right)_{s,1}}{\Delta\tau} = 0 \qquad \text{(C7)}$$

For $m = 1$, $n = L$, the equation is

$$\frac{\left(\frac{h_2}{h_1}k\right)_{1,L-\frac{3}{2}}\left(T_{1,L-1} - T_{1,L-2}\right)}{3\,\Delta x^2} - \frac{3\left(\frac{h_2}{h_1}k\right)_{1,L-\frac{1}{2}}\left(T_{1,L} - T_{1,L-1}\right)}{\Delta x^2}$$

$$+ \frac{3\left(\frac{h_2}{h_1}A\right)_{1,L-\frac{1}{2}}\left[\left(\delta\dot{m}_p\,\Delta h_p\right)_{1,L} + \left(\delta\dot{m}_p\,\Delta h_p\right)_{1,L-1}\right]}{2\,\Delta x}$$

$$- \frac{\left(\frac{h_2}{h_1}A\right)_{1,L-\frac{3}{2}}\left[\left(\delta\dot{m}_p\,\Delta h_p\right)_{1,L-1} + \left(\delta\dot{m}_p\,\Delta h_p\right)_{1,L-2}\right]}{6\,\Delta x}$$

$$+ \frac{1}{\delta_L{}^2}\left[\frac{3\left(h_1h_2k\right)_{\frac{3}{2},L}\left(T_{2,L} - T_{1,L}\right)}{\Delta\eta^2} - \frac{\left(h_1h_2k\right)_{\frac{5}{2},L}\left(T_{3,L} - T_{2,L}\right)}{3\,\Delta\eta^2} - \frac{8}{3\,\Delta\eta}\left(h_1h_2\delta\dot{m}_p\,\Delta h_p\right)_{1,L}\right]$$

$$- \frac{\left(h_1h_2\dot{m}_y\right)_{1,L}}{\delta_L}\,\frac{4\left(\bar{c}_pT\right)_{2,L} - \left(\bar{c}_pT\right)_{3,L} - 3\left(\bar{c}_pT\right)_{1,L}}{2\,\Delta\eta}$$

$$- \left[\frac{h_1h_2\rho c_p\dot{m}_p}{(\rho' - \rho)\delta}\right]_{1,L}\,\frac{4T_{2,L} - T_{3,L} - 3T_{1,L}}{2\,\Delta\eta}$$

$$- \left(h_1h_2\rho c_p\right)_{1,L}\,\frac{T_{1,L} - \left(T_o\right)_{1,L}}{\Delta\tau} = 0 \qquad \text{(C8)}$$

For $m = s$, $n = L$, the equation is

$$\frac{\left(\frac{h_2}{h_1}k\right)_{s,L-\frac{3}{2}}\left(T_{s,L-1} - T_{s,L-2}\right)}{3\,\Delta x^2} - \frac{3\left(\frac{h_2}{h_1}k\right)_{s,L-\frac{1}{2}}\left(T_{s,L} - T_{s,L-1}\right)}{\Delta x^2}$$

$$+ \frac{3\left(\frac{h_2}{h_1}A\right)_{s,L-\frac{1}{2}}\left[\delta_L\left(q_t\sigma\epsilon T^4\right)_{s,L} + \delta_{L-1}\left(q_t - \sigma\epsilon T^4\right)_{s,L-1}\right]}{2\,\Delta x}$$

$$- \frac{\left(\frac{h_2}{h_1}A\right)_{s,L-\frac{3}{2}}\left[\delta_{L-1}\left(q_t - \sigma\epsilon T^4\right)_{s,L-1} + \delta_{L-2}\left(q_t - \sigma\epsilon T^4\right)_{s,L-2}\right]}{6\,\Delta x}$$

$$+ \frac{1}{\delta_L{}^2}\left[\frac{\left(h_1h_2k\right)_{s-\frac{3}{2},L}\left(T_{s-1,L} - T_{s-2,L}\right)}{3\,\Delta\eta^2} - \frac{3\left(h_1h_2k\right)_{s-\frac{1}{2},L}\left(T_{s,L} - T_{s-1,L}\right)}{\Delta\eta^2}\right.$$

$$\left. + \frac{8}{3\,\Delta\eta}\left(h_1h_2\delta\right)_{s,L}\left(q_t - \sigma\epsilon T^4\right)_{s,L}\right]$$

$$- \frac{\left(h_1h_2\dot{m}_y\right)_{s,L}}{\delta_L}\,\frac{\left(\bar{c}_pT\right)_{s-2,L} + 3\left(\bar{c}_pT\right)_{s,L} - 4\left(\bar{c}_pT\right)_{s-1,L}}{2\,\Delta\eta}$$

$$- \left(\frac{h_1h_2c_p\dot{m}_c}{\delta}\right)_{s,L}\,\frac{3T_{s,L} + T_{s-2,L} - 4T_{s-1,L}}{2\,\Delta\eta}$$

$$- \left(h_1h_2\rho c_p\right)_{s,L}\,\frac{T_{s,L} - \left(T_o\right)_{s,L}}{\Delta\tau} = 0 \qquad \text{(C9)}$$

Pressure Equations

The finite-difference equations for the pressure distribution in the char layer are as follows:

For $1 < m < s$, $1 < n < L$, the equation is

$$\frac{\left(\frac{h_2}{h_1}\varphi\right)_{m,n+\frac{1}{2}} p^2_{m,n+1} - \left[\left(\frac{h_2}{h_1}\varphi\right)_{m,n+\frac{1}{2}} + \left(\frac{h_2}{h_1}\varphi\right)_{m,n-\frac{1}{2}}\right] p^2_{m,n} + \left(\frac{h_2}{h_1}\varphi\right)_{m,n-\frac{1}{2}} p^2_{m,n-1}}{\Delta x^2}$$

$$- \frac{\left(\frac{h_2}{h_1}\varphi A\right)_{m,n+1}\left(p^2_{m+1,n+1} - p^2_{m-1,n+1}\right) - \left(\frac{h_2}{h_1}\varphi A\right)_{m,n-1}\left(p^2_{m+1,n-1} - p^2_{m-1,n-1}\right)}{4\,\Delta\eta\,\Delta x}$$

$$- A_{m,n} \frac{\left(\frac{h_2}{h_1}\varphi\right)_{m+1,n}\left(p^2_{m+1,n+1} - p^2_{m+1,n-1}\right) - \left(\frac{h_2}{h_1}\varphi\right)_{m-1,n}\left(p^2_{m-1,n+1} - p^2_{m-1,n-1}\right)}{4\,\Delta\eta\,\Delta x}$$

$$+ A_{m,n} \frac{\left(\frac{h_2}{h_1}\varphi A\right)_{m+\frac{1}{2},n} p^2_{m+1,n} - \left[\left(\frac{h_2}{h_1}\varphi A\right)_{m+\frac{1}{2},n} + \left(\frac{h_2}{h_1}\varphi A\right)_{m-\frac{1}{2},n}\right] p^2_{m,n} + \left(\frac{h_2}{h_1}\varphi A\right)_{m-\frac{1}{2},n} p^2_{m-1,n}}{\Delta\eta^2}$$

$$+ \frac{1}{\delta_n{}^2} \frac{\left(h_1h_2\varphi\right)_{m+\frac{1}{2},n} p^2_{m+1,n} - \left[\left(h_1h_2\varphi\right)_{m+\frac{1}{2},n} + \left(h_1h_2\varphi\right)_{m-\frac{1}{2},n}\right] p^2_{m,n} + \left(h_1h_2\varphi\right)_{m-\frac{1}{2},n} p^2_{m-1,n}}{\Delta\eta^2}$$

$$- \left(\frac{h_1h_2f\eta\dot{m}_c}{\delta\rho}\right)_{m,n} \frac{\left(\rho_g\right)_{m+1,n} - \left(\rho_g\right)_{m-1,n}}{2\,\Delta\eta} - \left[\frac{h_1h_2f(1-\eta)\dot{m}_p}{\delta(\rho' - \rho)}\right]_{m,n} \frac{\left(\rho_g\right)_{m+1,n} - \left(\rho_g\right)_{m-1,n}}{2\,\Delta\eta}$$

$$- \left(h_1h_2f\right)_{m,n} \frac{\left(\rho_g\right)_{m,n} - \left(\rho_{g,o}\right)_{m,n}}{\Delta\tau} = 0$$

For $m = 1$, $1 < n < L$, the equation is:

$$\frac{\left(\frac{h_2}{h_1}\varphi\right)_{1,n+\frac{1}{2}} p^2_{1,n+1} - \left[\left(\frac{h_2}{h_1}\varphi\right)_{1,n+\frac{1}{2}} + \left(\frac{h_2}{h_1}\varphi\right)_{1,n-\frac{1}{2}}\right] p^2_{1,n} + \left(\frac{h_2}{h_1}\varphi\right)_{1,n-\frac{1}{2}} p^2_{1,n-1}}{\Delta x^2}$$

$$+ \frac{\left(\frac{h_2}{h_1} A\dot{m}_p \delta\right)_{1,n+1} - \left(\frac{h_2}{h_1} A\dot{m}_p \delta\right)_{1,n-1}}{2\,\Delta x}$$

$$- A_{1,n}\left[\frac{\left(\frac{h_2}{h_1}\varphi\right)_{2,n}\left(p^2_{2,n+1} - p^2_{2,n-1}\right)}{\Delta\eta\,\Delta x} - \frac{\left(\frac{h_2}{h_1}\varphi\right)_{3,n}\left(p^2_{3,n+1} - p^2_{3,n-1}\right)}{4\,\Delta\eta\,\Delta x} - \frac{3\left(\frac{h_2}{h_1}\varphi\right)_{1,n}\left(p^2_{1,n+1} - p^2_{1,n-1}\right)}{4\,\Delta\eta\,\Delta x}\right]$$

$$+ A_{1,n}\left[\frac{3\left(\frac{h_2}{h_1}\varphi A\right)_{\frac{3}{2},n}\left(p^2_{2,n} - p^2_{1,n}\right)}{\Delta\eta^2} - \frac{\left(\frac{h_2}{h_1}\varphi A\right)_{\frac{5}{2},n}\left(p^2_{3,n} - p^2_{2,n}\right)}{3\,\Delta\eta^2} + \frac{8}{3\,\Delta\eta}\left(\frac{h_2}{h_1} A\dot{m}_p \delta\right)_{1,n}\right]$$

$$+ \frac{1}{\delta_n{}^2}\left[\frac{3\left(h_1h_2\varphi\right)_{\frac{3}{2},n}\left(p^2_{2,n} - p^2_{1,n}\right)}{\Delta\eta^2} - \frac{\left(h_1h_2\varphi\right)_{\frac{5}{2},n}\left(p^2_{3,n} - p^2_{2,n}\right)}{3\,\Delta\eta^2} + \frac{8}{3\,\Delta\eta}\left(h_1h_2\dot{m}_p\delta\right)_{1,n}\right]$$

$$- \left[\frac{h_1h_2f\dot{m}_p}{\delta(\rho' - \rho)}\right]_{1,n} \frac{4(\rho_g)_{2,n} - (\rho_g)_{3,n} - 3(\rho_{g,1})_{1,n}}{2\,\Delta\eta}$$

$$- \left(h_1h_2f\right)_{1,n} \frac{(\rho_g)_{1,n} - (\rho_{g,o})_{1,n}}{\Delta\tau} = 0$$

For $m = s$, $1 < n < L$, $p^2_{s,n} = p^2_{e_{s,n}}$. For $1 < m < s$, $n = 1$, the equation is

$$\frac{6\left(\frac{\varphi}{h_1}\right)_{m,\frac{3}{2}}\left(p^2_{m,2} - p^2_{m,1}\right)}{\Delta x^2} - \frac{2\left(\frac{\varphi}{h_1}\right)_{m,\frac{5}{2}}\left(p^2_{m,3} - p^2_{m,2}\right)}{3\,\Delta x^2}$$

$$- \frac{3\left(\frac{\varphi A}{h_1}\right)_{m,\frac{3}{2}}\left[\left(p^2_{m+1,1} - p^2_{m-1,1}\right) + \left(p^2_{m+1,2} - p^2_{m-1,2}\right)\right]}{2\,\Delta\eta\,\Delta x}$$

$$+ \frac{\left(\frac{\varphi A}{h_1}\right)_{m,\frac{5}{2}}\left[\left(p^2_{m+1,2} - p^2_{m-1,2}\right) + \left(p^2_{m+1,3} - p^2_{m-1,3}\right)\right]}{6\,\Delta x\,\Delta\eta}$$

$$+ \frac{1}{\delta_1{}^2}\,\frac{\left(h_1\varphi\right)_{m+\frac{1}{2},1} p^2_{m+1,1} - \left[\left(h_1\varphi\right)_{m+\frac{1}{2},1} + \left(h_1\varphi\right)_{m-\frac{1}{2},1}\right] p^2_{m,1} + \left(h_1\varphi\right)_{m-\frac{1}{2},1} p^2_{m-1,1}}{\Delta\eta^2}$$

$$+ \left(\frac{\varphi}{R\delta}\right)_{m,1}\frac{p^2_{m+1,1} - p^2_{m-1,1}}{2\,\Delta\eta} - \left(\frac{h_1 f \eta \dot{m}_c}{\delta\rho}\right)_{m,1}\frac{\left(\rho_g\right)_{m+1,1} - \left(\rho_g\right)_{m-1,1}}{2\,\Delta\eta}$$

$$- \left[\frac{h_1 f(1-\eta)\dot{m}_p}{\delta(\rho' - \rho)}\right]_{m,1}\frac{\left(\rho_g\right)_{m+1,1} - \left(\rho_g\right)_{m-1,1}}{2\,\Delta\eta} - \left(h_1 f\right)_{m,1}\frac{\left(\rho_g\right)_{m,1} - \left(\rho_{g,o}\right)_{m,1}}{\Delta\tau} = 0 \qquad \text{(C12)}$$

For $1 < m < s$, $n = L$, the equation is

$$\frac{\left(\frac{h_2}{h_1}\varphi\right)_{m,L-\frac{3}{2}}\left(p^2_{m,L-1} - p^2_{m,L-2}\right)}{3\,\Delta x^2} - \frac{3\left(\frac{h_2}{h_1}\varphi\right)_{m,L-\frac{1}{2}}\left(p^2_{m,L} - p^2_{m,L-1}\right)}{\Delta x^2}$$

$$+ \frac{3\left(\frac{h_2}{h_1}\varphi A\right)_{m,L-\frac{1}{2}}\left[\left(p^2_{m+1,L} - p^2_{m-1,L}\right) + \left(p^2_{m+1,L-1} - p^2_{m-1,L-1}\right)\right]}{4\,\Delta\eta\,\Delta x}$$

$$- \frac{\left(\frac{h_2}{h_1}\varphi A\right)_{m,L-\frac{5}{2}}\left[\left(p^2_{m+1,L-1} - p^2_{m-1,L-1}\right) + \left(p^2_{m+1,L-2} - p^2_{m-1,L-2}\right)\right]}{12\,\Delta\eta\,\Delta x}$$

$$+ \frac{1}{\delta_L^{\,2}}\frac{\left(h_1h_2\varphi\right)_{m+\frac{1}{2},L}p^2_{m+1,L}}{\Delta\eta^2} - \frac{\left[\left(h_1h_2\varphi\right)_{m+\frac{1}{2},L} + \left(h_1h_2\varphi\right)_{m-\frac{1}{2},L}\right]p^2_{m,L}}{\Delta\eta^2}$$

$$+ \frac{\left(h_1h_2\varphi\right)_{m-\frac{1}{2},L}p^2_{m-1,L}}{\Delta\eta^2} - \left(\frac{h_1h_2f\eta\dot{m}_c}{\delta p}\right)_{m,L}\frac{\left(\rho_g\right)_{m+1,L} - \left(\rho_g\right)_{m-1,L}}{2\,\Delta\eta}$$

$$- \left[\frac{h_1h_2f(1-\eta)\dot{m}_p}{\delta(\rho' - \rho)}\right]_{m,L}\frac{\left(\rho_g\right)_{m+1,L} - \left(\rho_g\right)_{m-1,L}}{2\,\Delta\eta}$$

$$- \left(h_1h_2f\right)_{m,L}\frac{\left(\rho_g\right)_{m,L} - \left(\rho_{g,o}\right)_{m,L}}{\Delta\tau} = 0 \qquad \text{(C13)}$$

For $m = 1$, $n = 1$, the equation is

$$\frac{6\left(\frac{\varphi}{h_1}\right)_{1,\frac{3}{2}}\left(p^2_{1,2} - p^2_{1,1}\right)}{\Delta x^2} - \frac{2\left(\frac{\varphi}{h_1}\right)_{1,\frac{5}{2}}\left(p^2_{1,3} - p^2_{1,2}\right)}{3\,\Delta x^2}$$

$$- \frac{3\left(\frac{\varphi A}{h_1}\right)_{1,\frac{3}{2}}\left[\left(\frac{\delta \dot{m}_p}{\varphi}\right)_{1,1} + \left(\frac{\delta \dot{m}_p}{\varphi}\right)_{1,2}\right]}{\Delta x}$$

$$+ \frac{\left(\frac{\varphi A}{h_1}\right)_{1,\frac{5}{2}}\left[\left(\frac{\delta \dot{m}_p}{\varphi}\right)_{1,2} + \left(\frac{\delta \dot{m}_p}{\varphi}\right)_{1,3}\right]}{3\,\Delta x}$$

$$+ \frac{1}{{\delta_1}^2}\left[\frac{3\left(h_1\varphi\right)_{\frac{3}{2},1}\left(p^2_{2,1} - p^2_{1,1}\right)}{\Delta \eta^2} - \frac{\left(h_1\varphi\right)_{\frac{5}{2},1}\left(p^2_{3,1} - p^2_{2,1}\right)}{3\,\Delta \eta^2} + \frac{8}{3\,\Delta \eta}\left(h_1 \delta \dot{m}_p\right)_{1,1}\right]$$

$$- \left(\frac{\dot{m}_p}{R}\right)_{1,1} - \left[\frac{h_1 f \dot{m}_p}{\delta(\rho' - \rho)}\right]_{1,1} \frac{4\left(\rho_g\right)_{2,1} - 3\left(\rho_g\right)_{1,1} - \left(\rho_g\right)_{3,1}}{2\,\Delta \eta}$$

$$- \left(h_1 f\right)_{1,1} \frac{\left(\rho_g\right)_{1,1} - \left(\rho_{g,o}\right)_{1,1}}{\Delta \tau} = 0 \qquad \text{(C14)}$$

For $m = 1$, $n = L$, the equation is

$$\frac{\left(\frac{h_2}{h_1}\varphi\right)_{1,L-\frac{3}{2}}\left(p^2_{1,L-1} - p^2_{1,L-2}\right)}{3\,\Delta x^2} - \frac{3\left(\frac{h_2}{h_1}\varphi\right)_{1,L-\frac{1}{2}}\left(p^2_{1,L} - p^2_{1,L-1}\right)}{\Delta x^2}$$

$$- \frac{3\left(\frac{h_2}{h_1}\varphi A\right)_{1,L-\frac{1}{2}}\left[\left(\frac{\delta\dot{m}_p}{\varphi}\right)_{1,L} + \left(\frac{\delta\dot{m}_p}{\varphi}\right)_{1,L-1}\right]}{2\,\Delta x}$$

$$+ \frac{\left(\frac{h_2}{h_1}\varphi A\right)_{1,L-\frac{3}{2}}\left[\left(\frac{\delta\dot{m}_p}{\varphi}\right)_{1,L-1} + \left(\frac{\delta\dot{m}_p}{\varphi}\right)_{1,L-2}\right]}{6\,\Delta x}$$

$$+ \frac{1}{\delta_L{}^2}\left[\frac{3\left(h_1h_2\varphi\right)_{\frac{3}{2},L}\left(p^2_{2,L} - p^2_{1,L}\right)}{\Delta\eta^2} - \frac{\left(h_1h_2\varphi\right)_{\frac{5}{2},L}\left(p^2_{3,L} - p^2_{2,L}\right)}{3\,\Delta\eta^2} + \frac{8}{3\,\Delta\eta}\left(h_1h_2\,\delta\dot{m}_p\right)_{1,L}\right]$$

$$- \left[\frac{h_1h_2f\dot{m}_p}{\delta(\rho' - \rho)}\right]_{1,L} \frac{4\left(\rho_g\right)_{2,L} - \left(\rho_g\right)_{3,L} - 3\left(\rho_g\right)_{1,L}}{2\,\Delta\eta}$$

$$- \left(h_1h_2f\right)_{1,L} \frac{\left(\rho_g\right)_{1,L} - \left(\rho_{g,o}\right)_{1,L}}{\Delta\tau} = 0 \qquad \text{(C15)}$$

Mass-Flow Equations

The finite-difference equations for the mass-flow distribution in the char layer are as follows:

Component in x-direction.- For $1 < m < s$, $1 < n < L$, the equation is

$$\left(\dot{m}_x\right)_{m,n} = -\left(\frac{\varphi}{h_1}\right)_{m,n}\left[\frac{p^2_{m,n+1} - p^2_{m,n-1}}{2\,\Delta x} - \frac{A_{m,n}\left(p^2_{m+1,n} - p^2_{m-1,n}\right)}{2\,\Delta\eta}\right] \tag{C16}$$

For $m = 1$, $1 < n < L$, the equation is

$$\left(\dot{m}_x\right)_{1,n} = -\left(\frac{\varphi}{h_1}\right)_{1,n}\left[\frac{p^2_{m,n+1} - p^2_{m,n-1}}{2\,\Delta x} + A_{1,n}\left(\frac{\dot{m}_p\delta}{\varphi}\right)_{1,n}\right] \tag{C17}$$

For $m = s$, $1 < n < L$, the equation is

$$\left(\dot{m}_x\right)_{s,n} = -\left(\frac{\varphi}{h_1}\right)_{s,n}\left\{\frac{\left(p_e^2\right)_{n+1} - \left(p_e^2\right)_{n-1}}{2\,\Delta x} - \frac{A_{s,n}\left[3\left(p_e^2\right)_n + p^2_{s-2,n} - 4p^2_{s-1,n}\right]}{2\,\Delta\eta}\right\} \tag{C18}$$

For $1 \leqq m \leqq s$, $n = 1$, and L, the equation is

$$\left(\dot{m}_x\right)_{m,1} = \left(\dot{m}_x\right)_{m,L} = 0 \tag{C19}$$

Component in y-direction.- For $1 < m < s$, $1 \leqq n \leqq L$, the equation is

$$\left(\dot{m}_y\right)_{m,n} = -\frac{\varphi_{m,n}}{\delta_n}\,\frac{p^2_{m+1,n} - p^2_{m-1,n}}{2\,\Delta\eta} \tag{C20}$$

For $m = 1$, $1 \leqq n \leqq L$, the equation is

$$\left(\dot{m}_y\right)_{1,n} = \left(\dot{m}_p\right)_n \tag{C21}$$

For $m = s$, $1 \leqq m \leqq L$, the equation is

$$\left(\dot{m}_y\right)_{s,n} = -\frac{\varphi_{s,n}}{\delta_n} \frac{3\left(p_e^2\right)_n - 4p^2_{s-1,n} + p^2_{s-2,n}}{2\,\Delta\eta} \tag{C22}$$

APPENDIX D

EXACT SOLUTIONS

Quasi-Steady-State Temperature Solution

An exact solution is obtained for a rectangular char layer undergoing quasi-steady-state ablation. Steady-state environmental conditions and constant material properties are used. Conditions are selected so that the char thickness is constant both in the x-direction and with time. Mass flow in the y-direction only is considered.

Under these conditions, the governing differential equation for the temperature distribution is

$$\frac{\partial^2 \overline{T}}{\partial x^2} + \frac{\partial^2 \overline{T}}{\partial y^2} + C \frac{\partial \overline{T}}{\partial y} = 0 \tag{D1}$$

where

$$\overline{T} = T - T_o$$

$$C = \frac{\dot{m}_p}{k}\left(\overline{c}_p + \frac{\rho c_p}{\rho' - \rho}\right) = \text{Constant}$$

The boundary conditions used are

$$\left.\begin{aligned} &\frac{\partial \overline{T}}{\partial x} = 0 && (x = 0;\quad x = L)\\ &\overline{T} = 0 && (y = 0)\\ &k \frac{\partial \overline{T}}{\partial y} = q_o \cos^2 \frac{\pi x}{2L} = \frac{q_o}{2}\left(1 + \cos \frac{\pi x}{L}\right) && (y = \delta) \end{aligned}\right\} \tag{D2}$$

The exact solution is

$$\overline{T} = \frac{q_o e^{-\frac{Cy}{2}}}{ke^{-\frac{C\delta}{2}}}\left(\frac{\sinh \frac{Cy}{2}}{Ce^{-\frac{C\delta}{2}}} + \frac{\cos \frac{\pi x}{L} \sinh \frac{By}{2}}{B \cosh \frac{B\delta}{2} - C \sinh \frac{B\delta}{2}}\right) \tag{D3}$$

where

$$B = \sqrt{C^2 + \frac{4\pi^2}{L^2}}$$

Pressure Solution for a Rectangle

An exact solution is obtained for the pressure distribution in a rectangular char layer with a steady-state surface pressure distribution and constant temperature. Under these conditions, the governing differential equation for the pressure distribution is

$$\frac{\partial^2 p^2}{\partial x^2} + \frac{\partial^2 p^2}{\partial y^2} = 0 \tag{D4}$$

The boundary conditions used are

$$\left.\begin{aligned} &\frac{\partial p^2}{\partial x} = 0 && (x = 0;\quad x = L)\\ &\frac{\partial p^2}{\partial y} = 0 && (y = 0)\\ &p^2 = p_t^2 \cos^2 \frac{\pi x}{2L} = \frac{p_t^2}{2}\left(1 + \cos \frac{\pi x}{L}\right) && (y = \delta) \end{aligned}\right\} \tag{D5}$$

The exact solution is

$$p^2 = \frac{p_t^2}{2}\left(1 + \cos \frac{\pi x}{L} \frac{\cosh \frac{\pi y}{L}}{\cosh \frac{\pi \delta}{L}}\right) \tag{D6}$$

The mass flow components are also calculated from the exact solution. Thus,

$$\left.\begin{aligned} \dot{m}_x &= -\varphi \frac{\partial p^2}{\partial x} = \varphi \frac{p_t^2}{2} \frac{\pi}{L} \sin \frac{\pi x}{L} \frac{\cosh \frac{\pi y}{L}}{\cosh \frac{\pi \delta}{L}}\\ \dot{m}_y &= -\varphi \frac{\partial p^2}{\partial y} = -\varphi \frac{p_t^2}{2} \frac{\pi}{L} \cos \frac{\pi x}{L} \frac{\sinh \frac{\pi y}{L}}{\cosh \frac{\pi \delta}{L}} \end{aligned}\right\} \tag{D7}$$

Spherical Pressure Distribution

An exact solution is obtained for the pressure distribution in a constant-thickness char layer on a spherical quadrant. A steady-state pressure distribution and constant temperature are used. Under these conditions, the governing differential equation for the pressure distribution is

$$\frac{\partial}{\partial r}\left(r^2 \frac{\partial p^2}{\partial r}\right) + \frac{1}{\sin \psi} \frac{\partial}{\partial \psi}\left(\sin \psi \frac{\partial p^2}{\partial \psi}\right) = 0 \tag{D8}$$

where r is a dimensionless radius $R_{\psi,r}/R_1$ and $1 \leqq r \leqq \frac{R_2}{R_1}$.

The boundary conditions used are

$$\left.\begin{aligned} &\frac{\partial p^2}{\partial \psi} = 0 && \left(\psi = 0; \quad \psi = \frac{\pi}{2}\right) \\ &\frac{\partial p^2}{\partial r} = 0 && (r = 1) \\ &p^2 = p_t{}^2 \cos^2 \psi && \left(r = \frac{R_2}{R_1}\right) \end{aligned}\right\} \tag{D9}$$

The exact solution is

$$p^2 = \frac{p_t{}^2}{3} + p_t{}^2\left(\cos^2 \psi - \frac{1}{3}\right) \frac{\left(\frac{R_{\psi,r}}{R_1}\right)^2 + \frac{2}{3}\left(\frac{R_1}{R_{\psi,r}}\right)^3}{\left(\frac{R_2}{R_1}\right)^2 + \frac{2}{3}\left(\frac{R_1}{R_2}\right)^3} \tag{D10}$$

The mass flow components are calculated from

$$\dot{m}_x = \dot{m}_\psi = -\frac{\varphi}{R_{\psi,r}} \frac{\partial p^2}{\partial \psi} = \frac{\partial \varphi}{R_{\psi,r}} p_t{}^2 \sin \psi \cos \psi \frac{\left(\frac{R_{\psi,r}}{R_1}\right)^2 + \frac{2}{3}\left(\frac{R_1}{R_{\psi,r}}\right)^3}{\left(\frac{R_2}{R_1}\right)^2 + \frac{2}{3}\left(\frac{R_1}{R_2}\right)^3} \tag{D11}$$

$$\dot{m}_y = \dot{m}_r = -\varphi \frac{\partial p^2}{\partial R_{\psi,r}} = -2\varphi p_t{}^2\left(\cos^2 \psi - \frac{1}{3}\right) \frac{\left(\frac{R_{\psi,r}}{R_1{}^2} - \frac{R_1{}^3}{R_{\psi,r}^4}\right)}{\left(\frac{R_2}{R_1}\right)^2 + \frac{2}{3}\left(\frac{R_1}{R_2}\right)^3} \tag{D12}$$

REFERENCES

1. Dow, Marvin B.; Bush, Harold G.; and Tompkins, Stephen S.: Analysis of the Supercircular Reentry Performance of a Low-Density Phenolic-Nylon Ablator. NASA TM X-1577, 1968.

2. Bush, Harold G.; and Dow, Marvin B.: Multidimensional Gas Flow Through Permeable Char Layers and Its Effects on Ablation. NASA TR R-296, 1969.

3. Swann, Robert T.; Pittman, Claud M.; and Smith, James C., Jr.: One-Dimensional Numerical Analysis of the Transient Response of Thermal Protection Systems. NASA TN D-2976, 1965.

4. Peterson, W. D.; and Spanier, J.: HOT-2: A Two-Dimensional Transient Heat Conduction Program for the CDC-6600. WAPD-TM-669, U.S. At. Energy Comm., June 1967.

5. McClure, John A.: TOODEE – A Two-Dimensional, Time-Dependent Heat Conduction Program. AEC Res. and Develop. Rep. IDO-17227, U.S. At. Energy Comm., Apr. 1967.

6. McCuen, Peter A.; Schaefer, John W.; Lundberg, Raymond E.; and Kendall, Robert M.: A Study of Solid-Propellant Rocket Motor Exposed Materials Behavior. AFRPL-TR-65-33, U.S. Air Force, Feb. 26, 1965.

7. Popper, L. A.; Toong, T. Y.; and Sutton, G. W.: Three-Dimensional Ablation Considering Shape Changes and Internal Heat Condition. AIAA Paper No. 70-199, Jan. 1970.

8. Moyer, Carl B.; Anderson, Larry W.; and Dahm, Thomas J.: A Coupled Computer Code for the Transient Thermal Response and Ablation of Non-Charring Heat Shields and Nose Tips. NASA CR-1630, 1970.

9. Friedman, H. A.; and McFarland, B. L.: Two-Dimensional Transient Ablation and Heat Conduction Analysis for Multimaterial Thrust Chamber Walls. J. Spacecraft Rockets, vol. 5, no. 7, July 1968, pp. 753-761.

10. Schneider, P. J.; Maurer, R. E.; and Strapp, M. G.: Two-Dimensional Transpiration-Cooled Nosetip. J. Spacecraft Rockets, vol. 8, no. 2, Feb. 1971, pp. 170-176.

11. Beckwith, Ivan E.: Similar Solutions for the Compressible Boundary Layer on a Yawed Cylinder With Transpiration Cooling. NASA TR R-42, 1959. (Supersedes NACA TN 4345.)

12. Muskat, M.: The Flow of Homogeneous Fluids Through Porous Media. First ed., second printing, J. W. Edwards, Inc., 1946.

13. Gavril, Bruce D.; and Lane, Frank: Finite Difference Equations and Their Solution for the Transient Temperature Distribution in Composite, Anisotropic, Generalized Bodies of Revolution. Tech. Rep. No. 230 (Contract No. NOrd 18053), Gen. Appl. Sci. Lab., Inc., May 26, 1961.

14. Douglas, Jim, Jr.: Alternating Direction Methods for Three Space Variables. Numer. Math., vol. 4, 1962, pp. 41-63.

15. Chao, B. T.: Selected Topics on Convective Heat Transfer. Advanced Heat Transfer, B. T. Chao, ed., Univ. Illinois Press, 1969, pp. 1-72.

16. Sokolnikoff, Ivan S.; and Sokolnikoff, Elizabeth S.: Higher Mathematics for Engineers and Physicists. Second ed., McGraw-Hill Book Co., Inc., 1941.

TABLE I.- COMPARISON OF EXACT AND CALCULATED QUASI-STEADY-STATE TEMPERATURE DISTRIBUTIONS

[Input values used were $q = 113.5\ kW/m^2$; $k = 0.624\ W/m\text{-}K$; $\delta = 0.06096\ m$; $L = 0.3048\ m$; $C = 3.2214\ 1/m$; $T_o = 556\ K$; $\Delta\eta = 0.25$ $(m = 5)$; $\Delta x = 0.0381\ m$ $(n = 9)$]

$$\text{Percent error} = \frac{T_{exact} - T_{calc}}{T_{exact}} \times 100$$

η	Percent error for x of –				
	0	0.25	0.5	0.75	1.0
1.0	0.242	0.237	0.215	0.143	0.009
.75	.275	.264	.228	.129	.023
.5	.274	.259	.209	.104	.020
.25	.277	.251	.183	.075	.025
0	.230	.200	.120	.050	-.020

TABLE II.- COMPARISON OF EXACT AND CALCULATED PRESSURE DISTRIBUTIONS FOR A RECTANGLE

[Input values used were $p_s = 105.336$ kN/m^2; $\delta = 0.06096$ m; $L = 0.3048$ m; $\Delta\eta = 0.25$ (m = 5); $\Delta x = 0.0381$ m (n = 9)]

$$\text{Percent error} = \frac{p_{exact} - p_{calc}}{p_{exact}} \times 100$$

η	Percent error for x^* of –				
	0	0.25	0.5	0.75	1.0
1.0	----	----	----	-----	-----
.75	0.000	0.015	0.000	-0.076	-0.070
.5	.009	.025	.000	-.125	-.180
.25	.014	.061	.000	-.142	-.178
0	.048	.036	.000	-.140	-.172

TABLE III.- COMPARISON BETWEEN EXACT AND CALCULATED MASS-FLOW-RATE DISTRIBUTIONS FOR A RECTANGLE

$$\left[\varphi = 7.76 \times 10^{-11}\ \mathrm{m^3/N\text{-}s}\right]$$

$$\text{Percent error} = \frac{\dot{m}_{exact} - \dot{m}_{calc}}{\dot{m}_{exact}} \times 100$$

(a) Percent error; x-component

η	Percent error for x of –				
	0	0.25	0.5	0.75	1.0
1.0	-	2.63	2.69	2.64	--
.75	-	2.49	2.49	2.50	--
.5	-	2.44	2.41	2.45	--
.25	-	2.42	2.36	2.42	--
0	-	2.42	2.35	2.42	--

(b) Percent error; y-component

η	Percent error for x of –				
	0	0.25	0.5	0.75	1.0
1.0	0.636	1.584	0.000	1.627	0.712
.75	-.122	.615	.000	.649	-.066
.5	.130	.660	.000	.683	.162
.25	-.371	.445	.000	.464	-.338
0	----	----	----	----	----

TABLE IV.- COMPARISON BETWEEN EXACT AND CALCULATED PRESSURE DISTRIBUTIONS FOR A HEMISPHERE

[Input values used were $p_s = 47.88\ N/m^2$; $R_1 = 0.06096$ m; $R_2 = 0.3048$ m; $\delta = 0.24384$ m; $L = 0.0957$ m; $\Delta\eta = 0.25$ (m = 5); $\Delta x = 0.0119$ m (n = 9)]

$$\text{Percent error} = \frac{p_{exact} - p_{calc}}{p_{exact}} \times 100$$

η	Percent error for x of –				
	0	0.079	0.157	0.236	0.314
1.0	----	-----	-----	-----	-----
.75	0.059	-0.14	-0.115	-0.029	-0.024
.5	-.638	-.619	-.352	.174	.477
.25	-.794	-.738	-.390	.086	.287
0	.028	-.045	-.154	-.281	-.359

TABLE V.- COMPARISON BETWEEN EXACT AND CALCULATED MASS FLOW DISTRIBUTIONS FOR A HEMISPHERE

$$\left[\varphi = 7.76 \times 10^{-11}\ m^3/N\text{-}s\right]$$

$$\text{Percent error} = \frac{\dot{m}_{exact} - \dot{m}_{calc}}{\dot{m}_{exact}} \times 100$$

(a) Percent error; x-component

η	Percent error for x of –				
	0	0.079	0.157	0.236	0.314
1.0	-	-0.418	0.075	0.568	----
.75	-	-.550	-.359	.441	----
.5	-	-3.17	-2.88	-2.30	----
.25	-	-6.13	-5.8	-4.92	----
0	-	2.64	.676	4.1	----

(b) Percent error; y-component

η	Percent error for x of –				
	0	0.079	0.157	0.236	0.314
1.0	-4.17	-0.890	-0.180	-2.03	-3.05
.75	3.06	2.66	3.32	1.46	1.87
.5	4.44	2.86	3.39	1.80	2.74
.25	-.932	-.676	.273	-1.46	-1.31
0	-----	-----	-----	----	----

TABLE VI.- MATERIAL PROPERTY VALUES USED IN CALCULATIONS FOR BODY SHAPES SHOWN IN FIGURE 5

k, W/m-K, for –	
278 K	0.156
833	0.156
1111	0.499
1389	1.217
1667	1.872
1944	2.652
2222	3.744
2500	4.742
2778	6.240
3056	7.675
$\bar{c}_p$, KJ/kg-K, for –	
278 K	3.64
833	3.35
1111	8.37
1389	13.60
1667	7.53
1944	4.39
2222	5.02
2778	9.20
3333	20.08
c_p, KJ/kg-K	2.26
Δh_p, MJ/kg	2.32
A_s, kg/m^2-s	4.88×10^{10}
B_s, K	4.25×10^4
A_i, kg/m^2-s	7.71×10^6
B_i, K	1.29×10^4
α_s	1.0
C_e	0.232
λ	0.75
ϵ	0.8
Δh_c, MJ/kg	10.0
μ, N-s/m^2	4.79×10^{-5}
M	20.0
κ_y, κ_x, m^2	9.29×10^{-12}
ρ, kg/m^3	256
ρ', kg/m^3	552
f	0.8

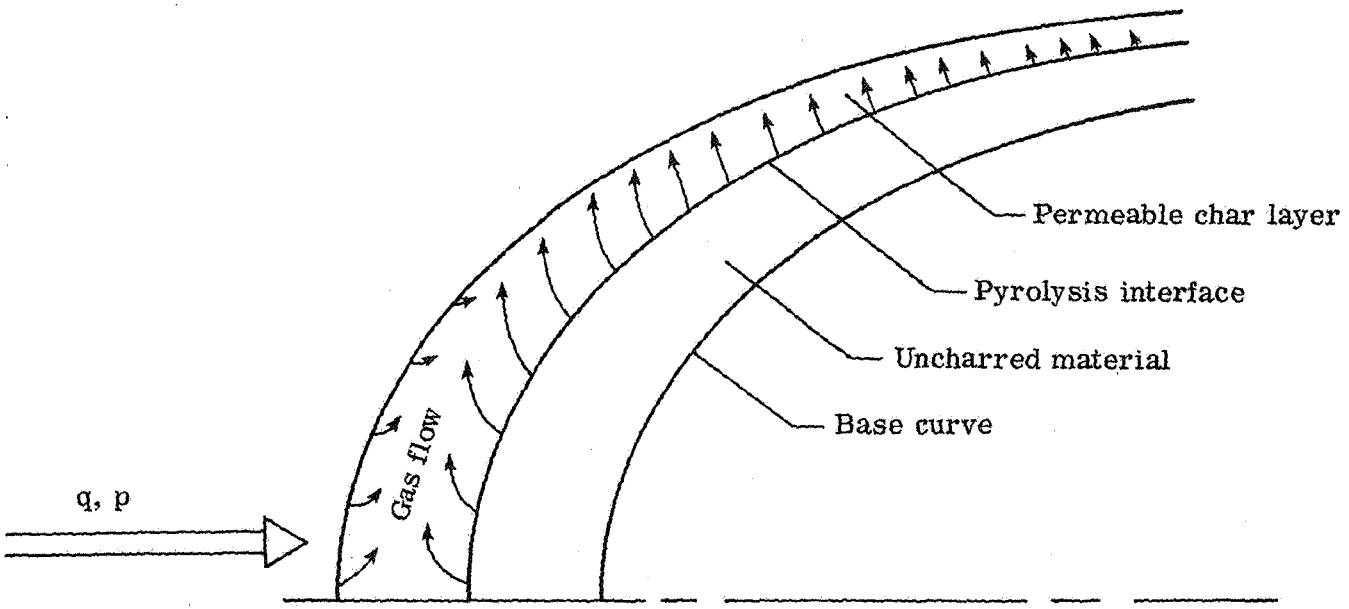

Figure 1.- Schematic of axisymmetric charring ablator.

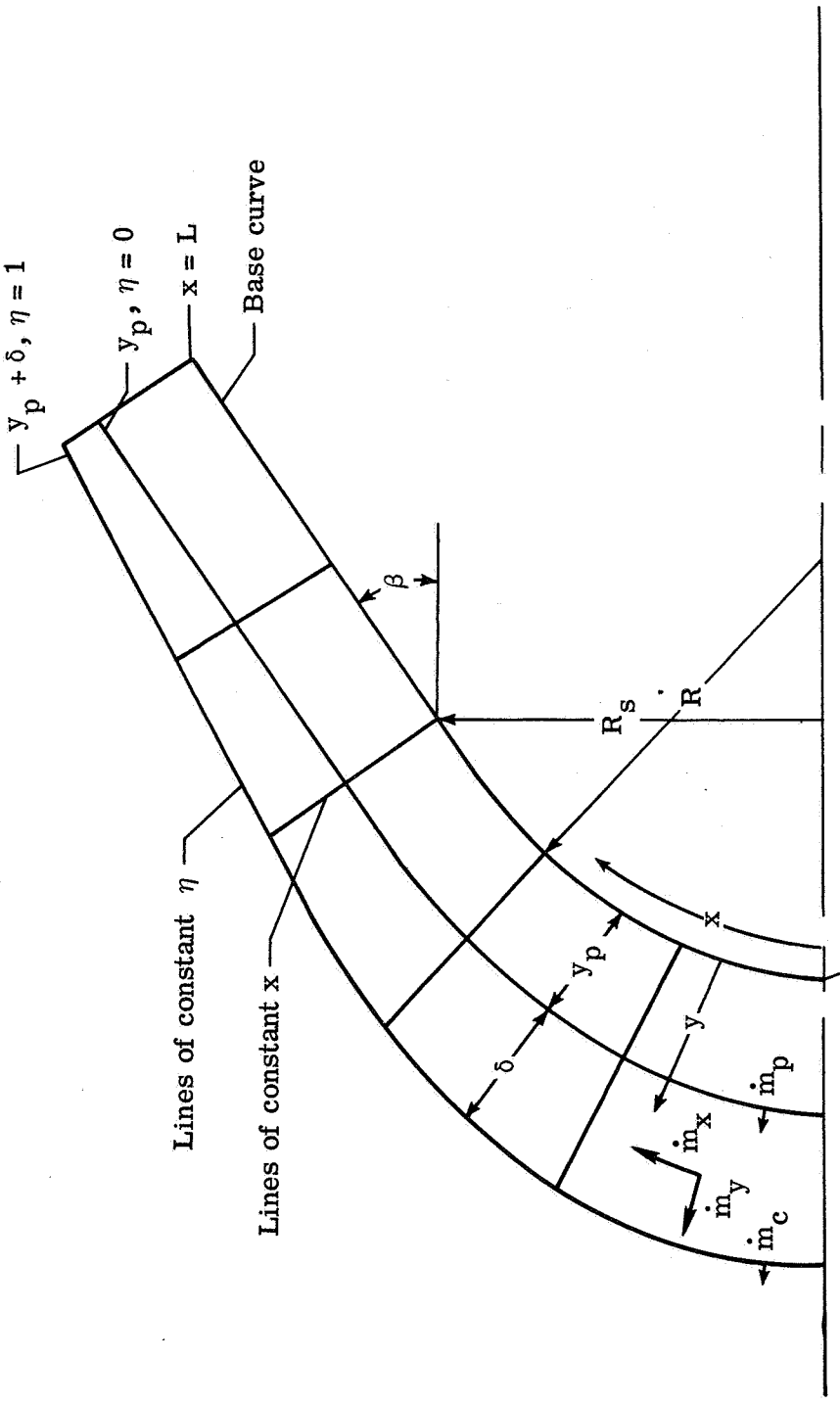

Figure 2.- Coordinate system.

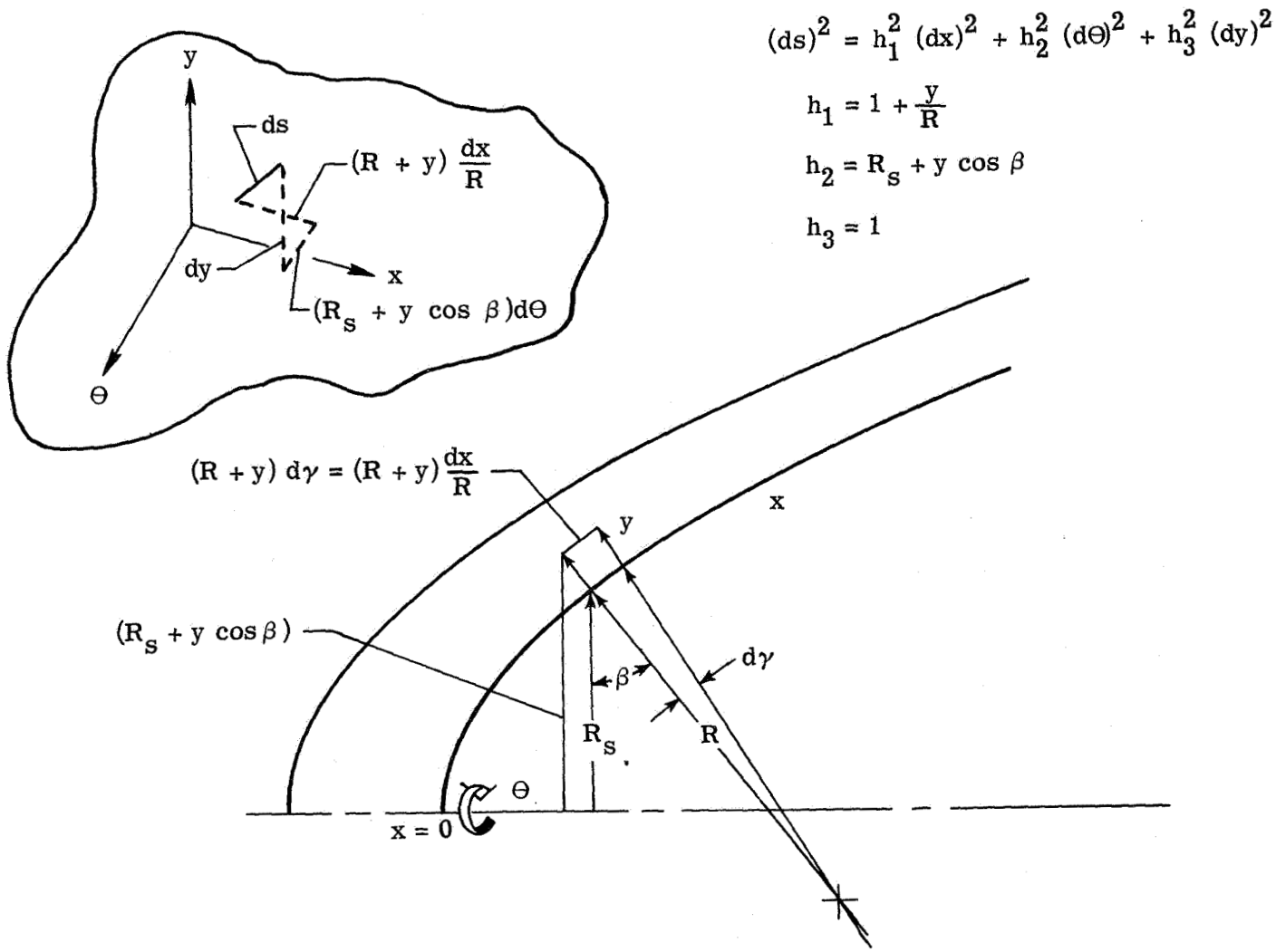

Figure 3.- Basic curvilinear coordinate system.

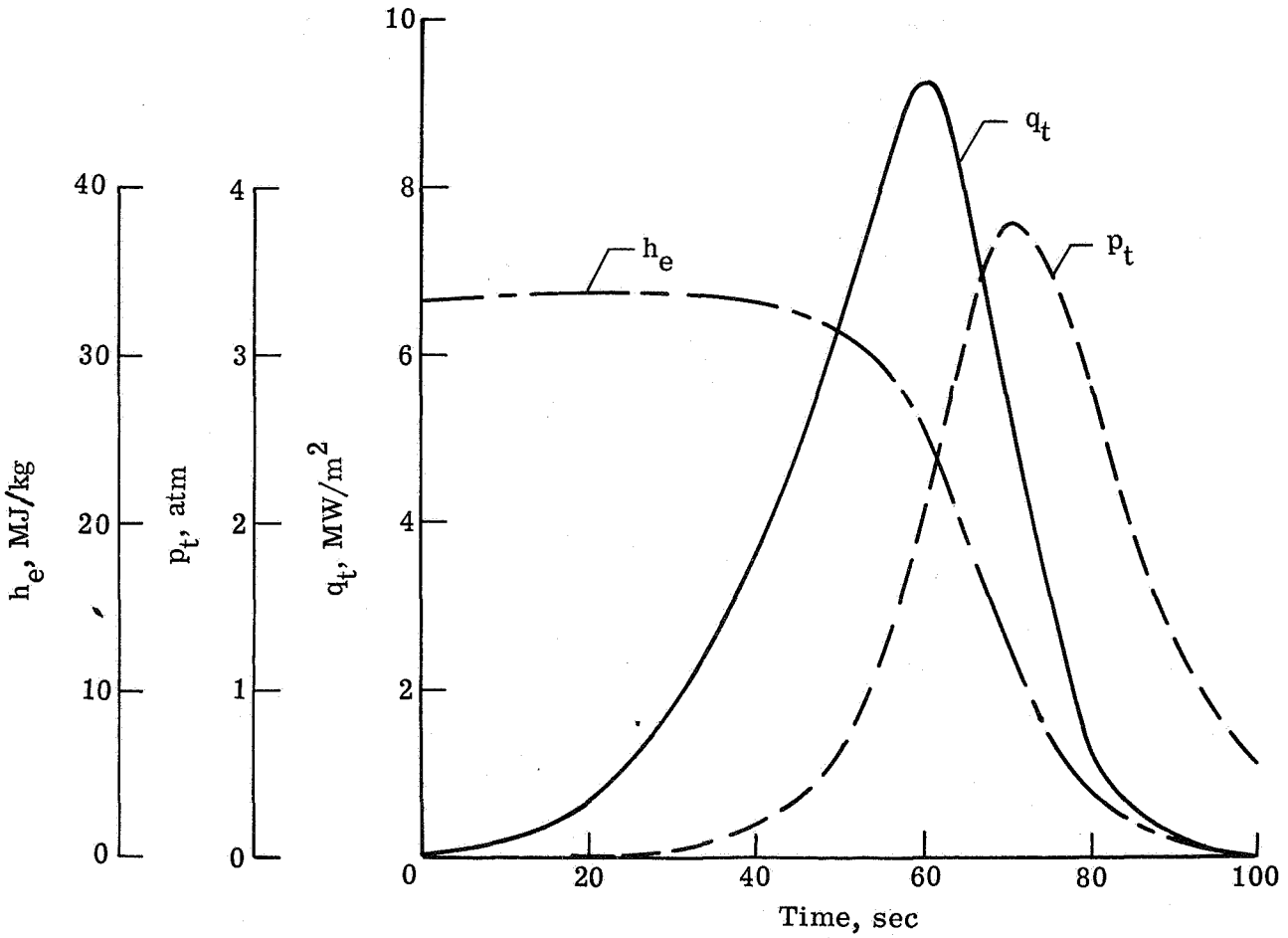

Figure 4.- Heating rate, pressure, and enthalpy histories used for typical calculated results.

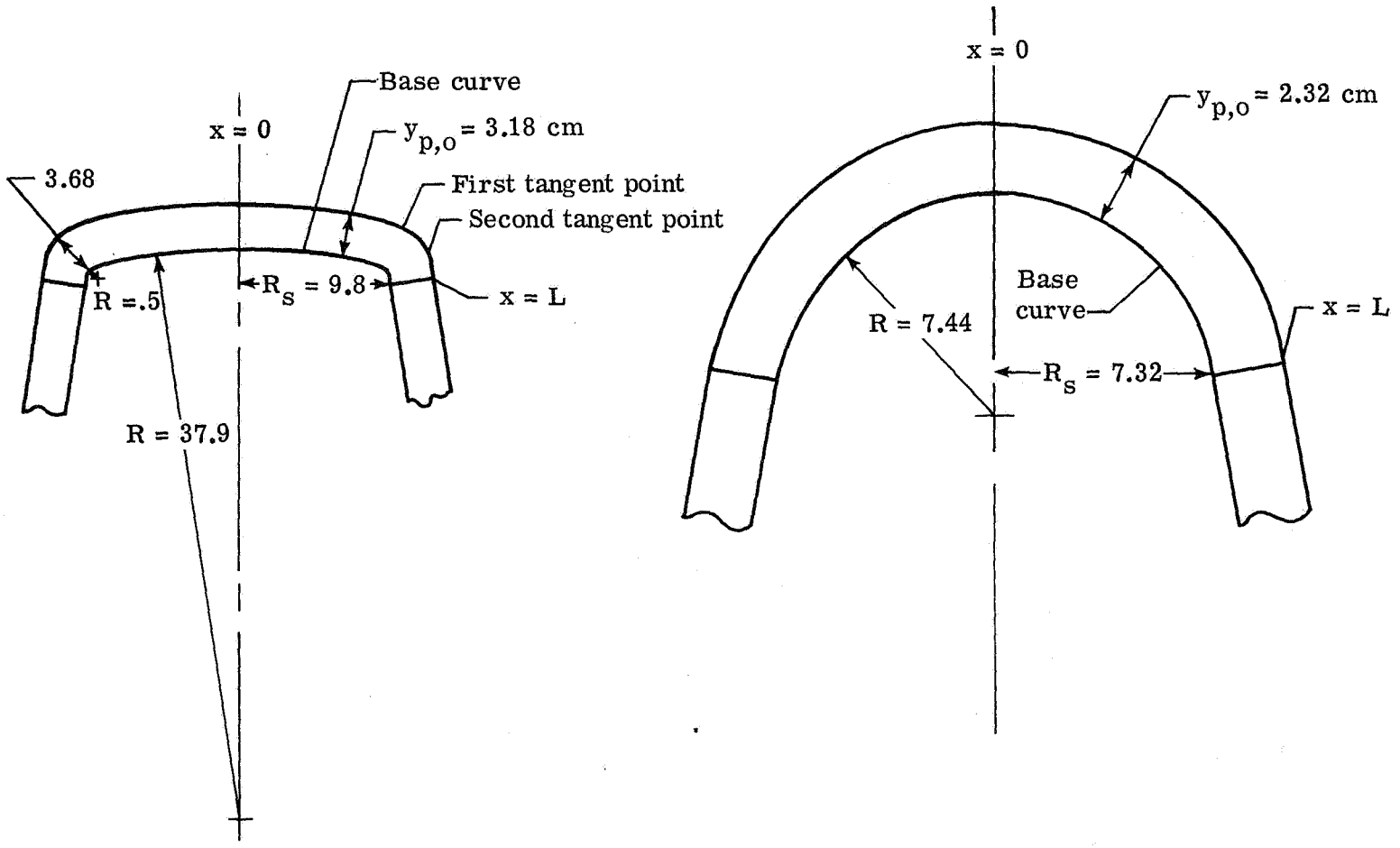

(a) Blunted cone.

(b) Hemisphere-cone.

Figure 5.- Axisymmetric shapes analyzed. All dimensions are in centimeters.

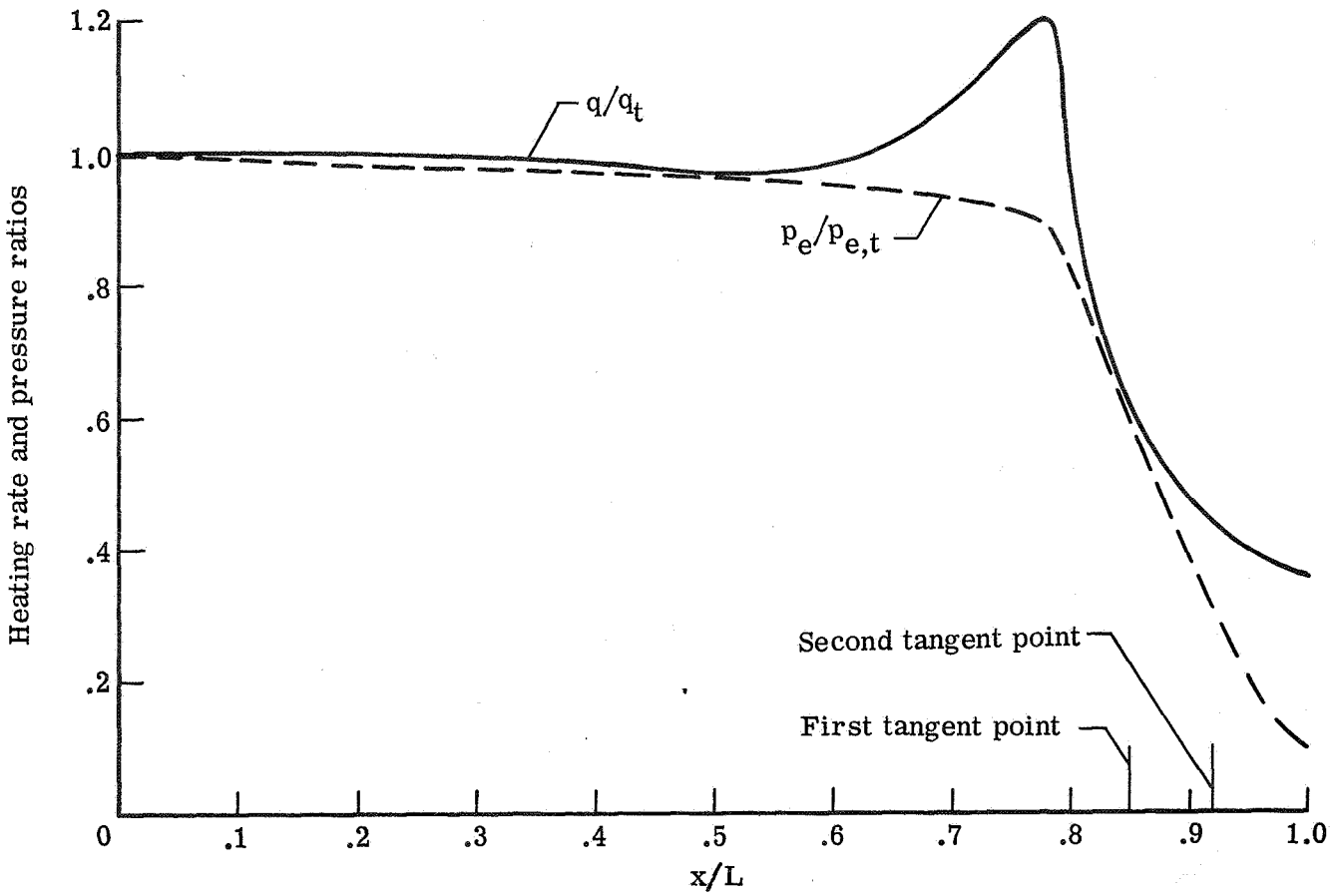

Figure 6.- Heating rate and pressure distributions for blunted cone.

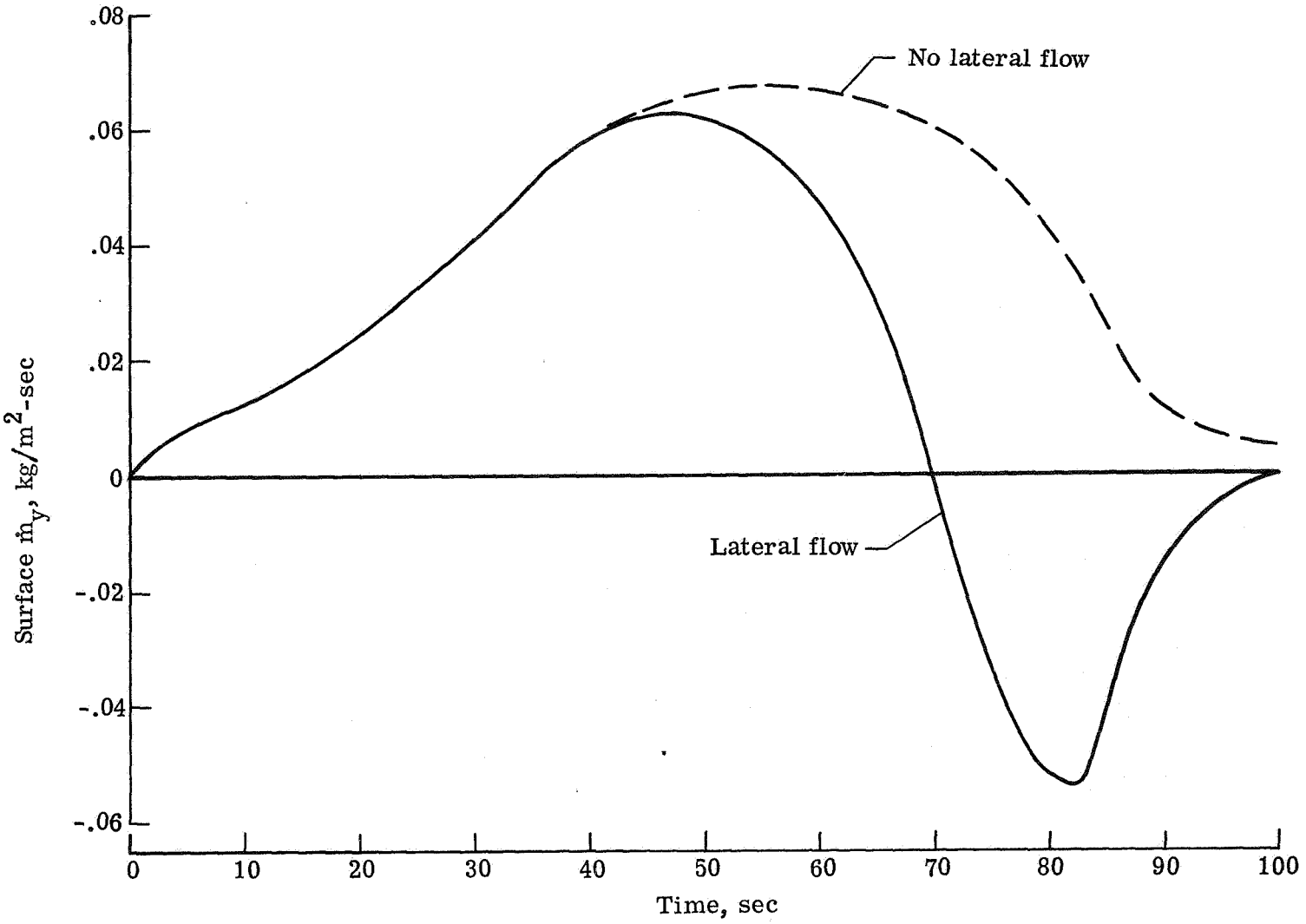

Figure 7.- Comparison of mass flow normal to surface, with and without lateral flow, at point of maximum two-dimensional effect. x/L = 0.78; blunted cone.

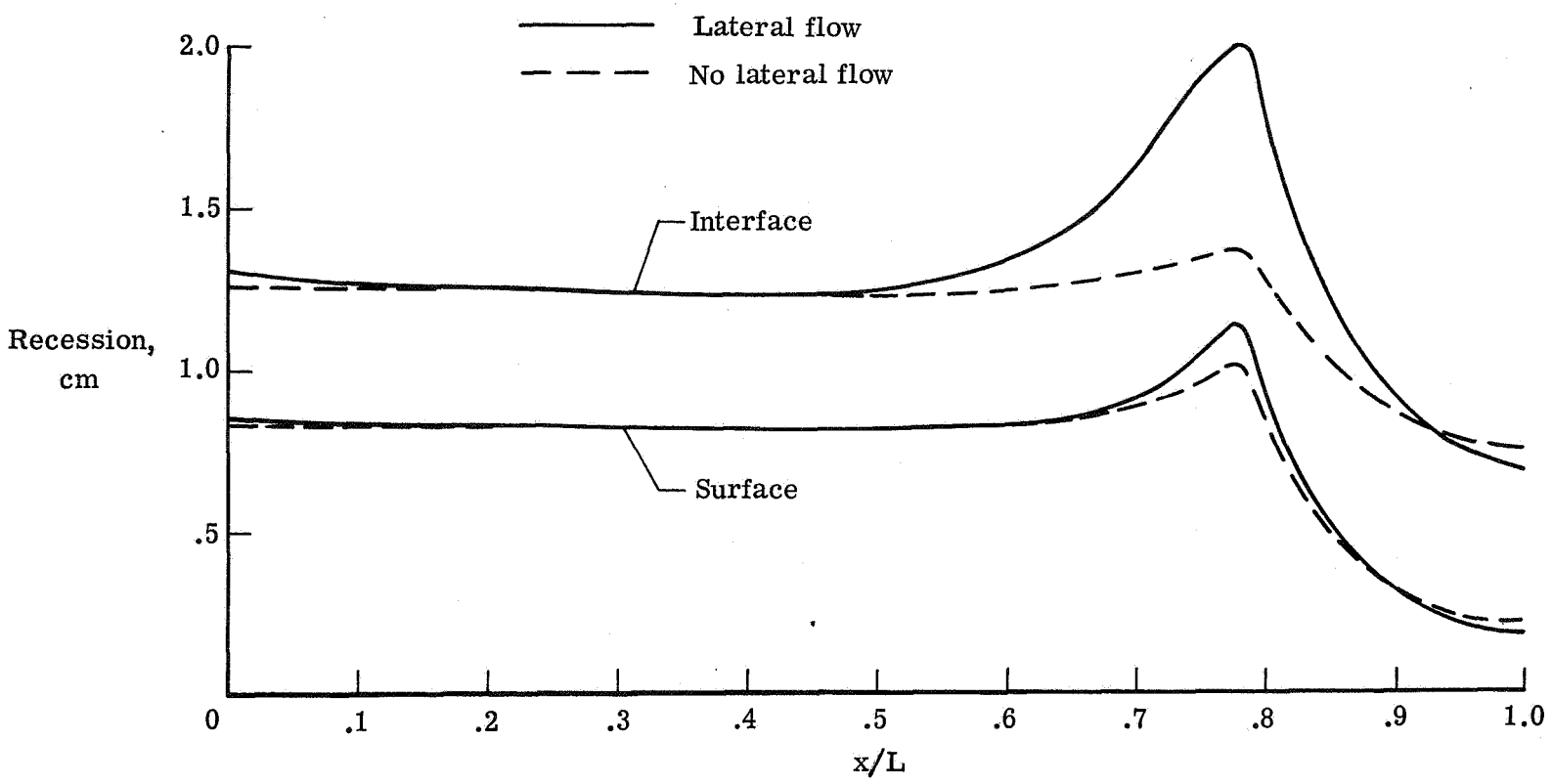

Figure 8.- Maximum surface and interface recessions. Blunted cone.

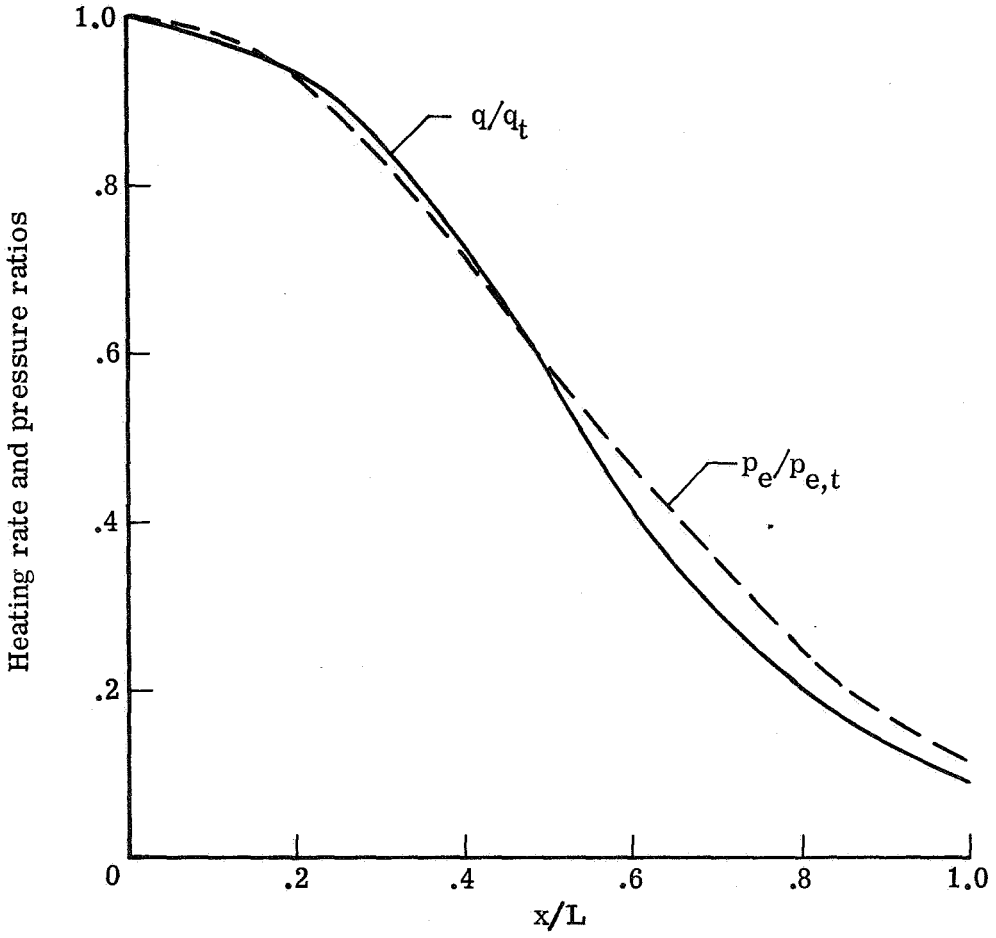

Figure 9.- Surface heating rate and pressure distributions for hemisphere-cone.

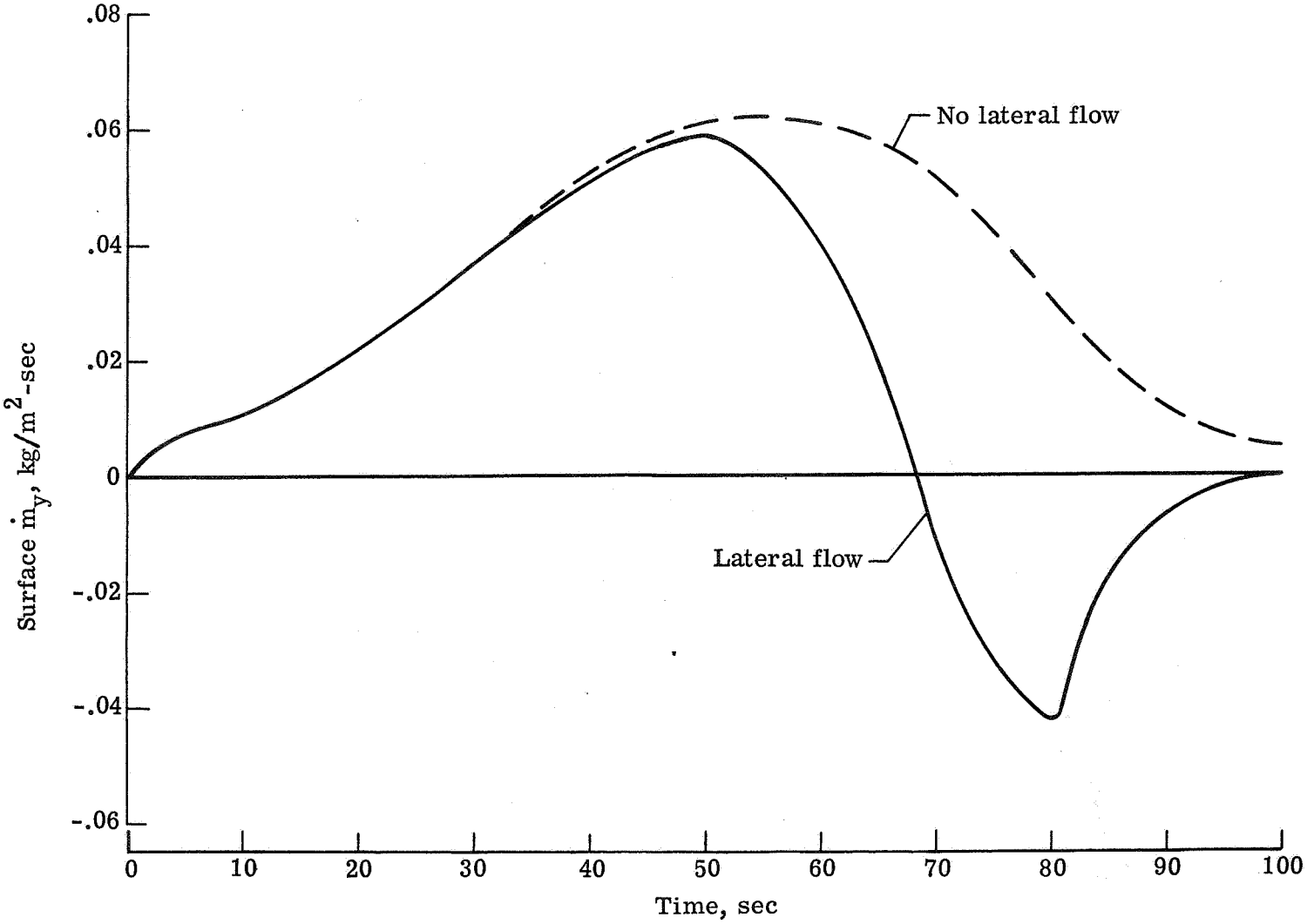

Figure 10.- Comparison of mass flow normal to surface, with and without lateral flow, at point of maximum two-dimensional effect. x = 0; hemisphere-cone.

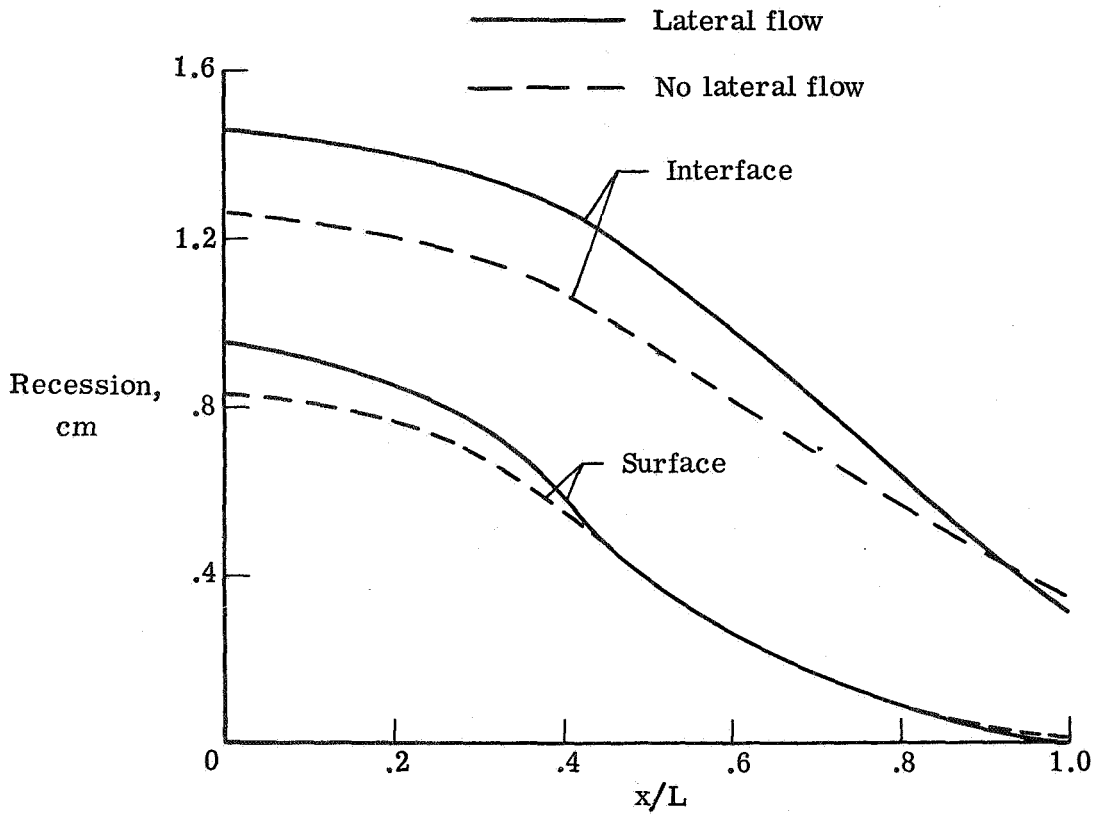

Figure 11.- Maximum surface and interface recessions. Hemisphere-cone.

NATIONAL AERONAUTICS AND SPACE ADMISTRATION
WASHINGTON, D.C. 20546

OFFICIAL BUSINESS
PENALTY FOR PRIVATE USE $300

FIRST CLASS MAIL

POSTAGE AND FEES PAID
NATIONAL AERONAUTICS AND
SPACE ADMINISTRATION

U.S.MAIL

NASA 451

POSTMASTER: If Undeliverable (Section 158 Postal Manual) Do Not Return

"The aeronautical and space activities of the United States shall be conducted so as to contribute . . . to the expansion of human knowledge of phenomena in the atmosphere and space. The Administration shall provide for the widest practicable and appropriate dissemination of information concerning its activities and the results thereof."

—NATIONAL AERONAUTICS AND SPACE ACT OF 1958

NASA SCIENTIFIC AND TECHNICAL PUBLICATIONS

TECHNICAL REPORTS: Scientific and technical information considered important, complete, and a lasting contribution to existing knowledge.

TECHNICAL NOTES: Information less broad in scope but nevertheless of importance as a contribution to existing knowledge.

TECHNICAL MEMORANDUMS: Information receiving limited distribution because of preliminary data, security classification, or other reasons.

CONTRACTOR REPORTS: Scientific and technical information generated under a NASA contract or grant and considered an important contribution to existing knowledge.

TECHNICAL TRANSLATIONS: Information published in a foreign language considered to merit NASA distribution in English.

SPECIAL PUBLICATIONS: Information derived from or of value to NASA activities. Publications include conference proceedings, monographs, data compilations, handbooks, sourcebooks, and special bibliographies.

TECHNOLOGY UTILIZATION PUBLICATIONS: Information on technology used by NASA that may be of particular interest in commercial and other non-aerospace applications. Publications include Tech Briefs, Technology Utilization Reports and Technology Surveys.

Details on the availability of these publications may be obtained from:

SCIENTIFIC AND TECHNICAL INFORMATION OFFICE

NATIONAL AERONAUTICS AND SPACE ADMINISTRATION

Washington, D.C. 20546